J. Fluid Mech. (1998), *vol.* 368, *pp.* 81–126. Printed in the United Kingdom

The lift force on a spherical bubble in a viscous linear shear flow

By DOMINIQUE LEGENDRE AND JACQUES MAGNAUDET

Institut de Mécanique des Fluides de Toulouse, UMR CNRS/INPT/UPS 5502,
2, Avenue Camille Soula, 31400 Toulouse, France

(Received 15 September 1997 and in revised form 10 March 1998)

The three-dimensional flow around a spherical bubble moving steadily in a viscous linear shear flow is studied numerically by solving the full Navier–Stokes equations. The bubble surface is assumed to be clean so that the outer flow obeys a zero-shear-stress condition and does not induce any rotation of the bubble. The main goal of the present study is to provide a complete description of the lift force experienced by the bubble and of the mechanisms responsible for this force over a wide range of Reynolds number ($0.1 \leqslant Re \leqslant 500$, Re being based on the bubble diameter) and shear rate ($0 \leqslant Sr \leqslant 1$, Sr being the ratio between the velocity difference across the bubble and the relative velocity). For that purpose the structure of the flow field, the influence of the Reynolds number on the streamwise vorticity field and the distribution of the tangential velocities at the surface of the bubble are first studied in detail. It is shown that the latter distribution which plays a central role in the production of the lift force is dramatically dependent on viscous effects. The numerical results concerning the lift coefficient reveal very different behaviours at low and high Reynolds numbers. These two asymptotic regimes shed light on the respective roles played by the vorticity produced at the bubble surface and by that contained in the undisturbed flow. At low Reynolds number it is found that the lift coefficient depends strongly on both the Reynolds number and the shear rate. In contrast, for moderate to high Reynolds numbers these dependences are found to be very weak. The numerical values obtained for the lift coefficient agree very well with available asymptotic results in the low- and high-Reynolds-number limits. The range of validity of these asymptotic solutions is specified by varying the characteristic parameters of the problem and examining the corresponding evolution of the lift coefficient. The numerical results are also used for obtaining empirical correlations useful for practical calculations at finite Reynolds number. The transient behaviour of the lift force is then examined. It is found that, starting from the undisturbed flow, the value of the lift force at short time differs from its steady value, even when the Reynolds number is high, because the vorticity field needs a finite time to reach its steady distribution. This finding is confirmed by an analytical derivation of the initial value of the lift coefficient in an inviscid shear flow. Finally, a specific investigation of the evolution of the lift and drag coefficients with the shear rate at high Reynolds number is carried out. It is found that when the shear rate becomes large, i.e. $Sr = O(1)$, a small but consistent decrease of the lift coefficient occurs while a very significant increase of the drag coefficient, essentially produced by the modifications of the pressure distribution, is observed. Some of the foregoing results are used to show that the well-known equality between the added mass coefficient and the lift coefficient holds only in the limit of weak shears and nearly steady flows.

1. Introduction

When a particle moves in a shear flow and more generally in a rotational flow, it experiences a transverse force. This force which is usually called the lift force is of major importance in many practical situations. It is for example essential for predicting the lateral distribution of bubbles in pipe flows: bubbles tend to migrate towards the wall in upward flows while they migrate towards the centre of the pipe when the flow goes downwards. The existence of the lift force for small rigid particles was first demonstrated experimentally by Segré & Silberberg (1962*a*, *b*) who studied the lateral migration of neutrally buoyant spheres in a Poiseuille flow. Because of its practical applications, the analytical calculation of the lift force on spherical particles has been a subject of constant interest for more than forty years. This calculation is very tedious even in asymptotic situations because it requires the consideration of the three-dimensional momentum equations without major simplifications. Actually two series of analytical work have been carried out on this problem. The first one considers the effect of an inviscid rotational flow on a sphere and was initiated by Lighthill (1956) and Hall (1956). Lighthill (1956) showed how the velocity field around the sphere can be estimated to a first approximation when the shear is weak. His method consists in evaluating how the incident vorticity is distorted by the potential flow induced by the presence of the sphere. His results were improved in several subsequent works, especially the one of Cousins (1970), but this author only obtained partial conclusions. Finally, Auton (1984, 1987) succeeded in performing the complete calculation of the secondary velocity field induced by the vorticity and evaluated the resulting lift force. His result was further extended to ellipsoids by Naciri (1992) who used a slightly different technique in order to avoid the calculation of a singular integral. The second series of work concerns low-Reynolds-number flows and is related to sedimentation problems. Combining several analytical techniques, Saffman (1965) obtained the lift force on a small rigid sphere in a linear shear flow in the limit of small Reynolds number and large shear. His solution is based on a matched asymptotic expansion in which the flow in the inner region is modified by the inertia effects induced by the shear in the outer region. McLaughlin (1991) extended Saffman's analysis by considering the case where inertia effects related to the mean flow are of same order as those induced by the shear. Recently, Legendre & Magnaudet (1997) reconsidered Saffman's and McLaughlin's analyses for a spherical drop of arbitrary viscosity. Their analytical solution is therefore valid for a spherical bubble with a vanishing viscosity. In that case the lift force was found to be $(2/3)^2$ times that of a solid sphere, the coefficient $2/3$ corresponding to the ratio of the magnitude of the vorticity at the surface of each kind of particle.

Several other flow situations involving a lift force have also been considered analytically for a sphere, namely the case of various high- or low-Reynolds-number two-dimensional shearing motions or the effect of a plane wall. Nevertheless they will not be discussed here because we shall devote specific papers to similar situations (see Magnaudet 1997 and Magnaudet & Legendre 1998 for a summary of the existing results concerning the case of shearing motions). In contrast another series of work deserves some lines of comments in view of the discussion below. It concerns the attempts made to evaluate the lift force on a sphere in an inviscid flow without explicitly solving the disturbed rotational flow around the sphere. The first step in that direction was probably carried out by Drew & Lahey (1979) who invoked the frame indifference principle in order to derive a general expression for the force density acting on a dilute suspension of spheres and concluded that the lift coefficient must equal the

added mass coefficient. Nevertheless, the various forms of the frame indifference principle and their validity were discussed in the context of forces acting upon particles by Ryskin & Rallison (1980) and Auton (1984). These authors showed that the form of that principle used by Drew & Lahey (1979) is generally incorrect, suggesting that their conclusions are invalid. Starting from very different grounds, Auton (1987) wrote a momentum balance on a large domain of fluid surrounding the sphere and concluded that, in the limit of weak shear rates, the lift coefficient C_L is equal to the entrained mass coefficient C_{VM} defined by Darwin (1953). Using a rotating frame of reference, Drew & Lahey (1987, 1990) considered the case of a sphere moving in an unsteady straining and rotating flow. In their initial (1987) paper they had concluded that the lift coefficient C_L was equal to the added mass coefficient C_M. Unfortunately their derivation involved a fundamental error and in their corrigendum (1990) they only concluded that the foregoing result holds for short times. More recently Zhang & Prosperetti (1994) derived a general expression of the force density acting on a suspension of spheres moving in a potential flow and generalized the result to a rotating frame. By requiring that this expression transforms in an objective way in a subsequent change of reference frame, they showed that a term identical to Auton's lift force appears when the flow is observed in a rotating frame. This brief summary shows that, even if the methodologies used by the previous groups of authors are different, their results converge in suggesting that the identity $C_L = C_M$ holds in inviscid flow. Moreover, it must be mentioned that this identity was also found to hold for ellipsoids by Naciri (1992), using a direct determination of the lift coefficient or a global momentum balance under assumptions similar to those of Auton (1987).

Compared to the amount of analytical work reviewed above, the number of computational studies that have considered the case of a spherical particle embedded in a shear flow is very small. Dandy & Dwyer (1990) obtained the first numerical estimates of the lift force on a rigid sphere for Reynolds numbers (based on the particle diameter and velocity at the centre of the sphere) ranging between 0.01 and 100. Nevertheless, their results display some troubling features. For example the flows they considered had a relatively low shear. Therefore, at the lowest Reynolds numbers that they studied, McLaughlin's approximations apply while Saffman's approximations do not. Despite this evidence their numerical predictions of the lift force were in good agreement with Saffman's solution but disagreed significantly with McLaughlin's result. Actually, as will be shown below, there are reasons to believe that the accuracy of the results of Dandy & Dwyer was strongly affected by the small size of their computational domain (25 sphere radii). Recently, Komori & Kurose (1996) and Kurose & Komori (1997) considered the same problem up to Reynolds numbers of several hundred. While the results of Dandy & Dwyer (1990) show that when the Reynolds number increases the lift coefficient (defined in a convenient manner) tends towards a constant positive value, those of Kurose & Komori display completely different trends: the latter authors find that beyond a certain Reynolds number the lift coefficient becomes negative and depends strongly on the shear rate. This brief summary shows that the situation concerning the lift force on a solid sphere is not clear at the present time, except in the low-Reynolds-number limit for which asymptotic results are available. This stresses the fact that the computation of the lift force is not a trivial matter because this force results from subtle distortions of the flow.

Concerning a clean spherical bubble, i.e. a sphere under a shear-free condition instead of a no-slip one, no computational study seems to have been reported up to now. One can of course argue that in most practical situations bubbles are neither clean nor spherical. The presence of surfactants on the surface of small spherical bubbles is

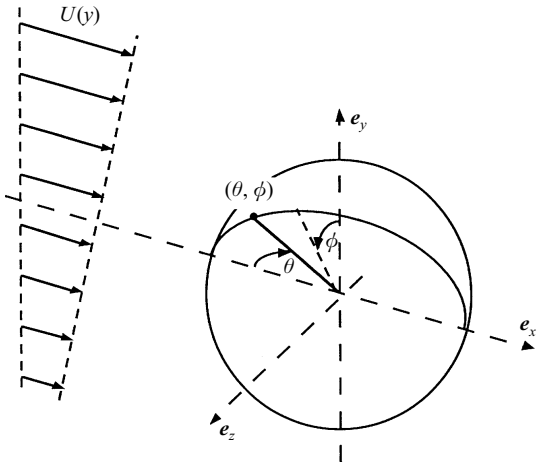

FIGURE 1. Sketch of the flow configuration.

known to produce interfacial shear stresses and therefore to increase the drag (see e.g. Cuenot, Magnaudet & Spennato 1997). It also has certainly a dramatic influence on the lift force because the amount of interfacial vorticity may be several orders of magnitude larger than for a clean interface. Regarding the effects of deformation, the computations performed by Ervin & Tryggvason (1994) and Takagi & Matsumoto (1995) for a deforming bubble moving in a shear flow revealed that the sign of the lift force can change when the bubble becomes significantly non-spherical. Thus, even for pure liquids, the results obtained for a spherical bubble may have a limited range of applicability. Despite these limitations, there is an intrinsic fundamental interest in the study of the lift force on a clean spherical bubble for the following reasons. First of all, the range of validity of the analytical solutions derived by Auton (1984, 1987) and by Legendre & Magnaudet (1997) is unknown and it is highly desirable to specify it in terms of Reynolds number and shear rate. Is the low-Reynolds-number asymptotic solution approximately valid for Reynolds numbers of order unity as is the Oseen's solution for the drag force? Similarly, beyond what Reynolds number and below what shear rate does Auton's solution apply in a viscous fluid? Then there is the question of the validity of the equality $C_L = C_M$. It has been shown in several previous numerical studies (see especially Rivero, Magnaudet & Fabre 1991, and Magnaudet, Rivero & Fabre 1995 for the case of bubbles) that the added mass coefficient of a sphere is a true constant and is in particular independent of the magnitude of the acceleration. Does the same result hold at high Reynolds number for the lift coefficient? Is this result also valid in transient situations? Finally, in contrast to the case of a solid sphere for which the vorticity produced by the no-slip condition increases continuously with the Reynolds number, two asymptotic solutions involving different physical mechanisms are available for a bubble. The supplementary asymptotic information valid in the limit of very high Reynolds number, i.e. Auton's theory, leads to the question of the general physical origin of the lift force: what are the ingredients required for obtaining a non-zero lift force at finite Reynolds number?

The present paper tries to provide some answers to the foregoing questions. For that purpose the lift force is computed by means of direct numerical simulations of the full Navier–Stokes equations. The numerical predictions are compared with the available analytical solutions at both low and high Reynolds number. Steady values of the lift and drag forces are presented for a wide range of Reynolds number and for two

moderate shear rates. At low and high Reynolds number, higher shear rates are considered in order to determine the range of validity of the analytical solutions mentioned above. The transient flow solutions obtained before the steady state is reached are also discussed in order to investigate the relaxation effects that may affect the lift force. The paper is organized as follows. The problem and the non-dimensional coefficients are defined in §2. Section 3 is devoted to a short presentation of the numerical code and to careful numerical tests. The results obtained for the flow field and the hydrodynamic forces are presented and discussed in §§4 and 5, respectively. The transient behaviour of the lift force is studied specifically in §6 while §7 discusses the evolution of this force at high Reynolds number when the shear rate increases. Finally §8 addresses the question of the relation between the lift coefficient and the added mass coefficient.

2. Statement of the problem

Let us consider a fixed spherical bubble of radius R located at the origin of a Cartesian frame of reference $(\boldsymbol{e}_x, \boldsymbol{e}_y, \boldsymbol{e}_z)$. The bubble is embedded in a steady linear shear flow (figure 1) corresponding to the undisturbed velocity field

$$\boldsymbol{U} = (U_o + \alpha y)\,\boldsymbol{e}_x. \tag{1}$$

The outer fluid is assumed to be Newtonian and its local velocity and pressure are denoted by $\boldsymbol{V}$ and P, respectively. The incompressible flow around the bubble is then governed by the full Navier–Stokes equations

$$\boldsymbol{\nabla}\cdot\boldsymbol{V} = 0, \quad \frac{\partial \boldsymbol{V}}{\partial t} + \boldsymbol{V}\cdot\boldsymbol{\nabla}\boldsymbol{V} = -\frac{1}{\rho}\boldsymbol{\nabla}P + \boldsymbol{\nabla}\cdot\boldsymbol{\tau}, \tag{2a,b}$$

where $\boldsymbol{\tau} = \nu(\boldsymbol{\nabla}\boldsymbol{V} + {}^t\boldsymbol{\nabla}\boldsymbol{V})$ is the viscous part of the stress tensor $\boldsymbol{\Sigma} = -P\boldsymbol{I} + \rho\boldsymbol{\tau}$, ρ and ν denoting the density and the kinematic viscosity of the fluid, respectively.

The boundary condition far from the bubble is obviously

$$\boldsymbol{V} \to \boldsymbol{U} \quad \text{for} \quad r \to \infty, \tag{3a}$$

where $r = (x^2 + y^2 + z^2)^{1/2}$. On the bubble surface the normal velocity must vanish, owing to the impermeability condition. Moreover, the dynamic viscosity of the gas filling the bubble is assumed to be negligible with respect to that of the surrounding fluid and the bubble surface is supposed to be free of any surfactant. Under these assumptions the boundary conditions on the bubble surface are:

$$\left.\begin{aligned} \boldsymbol{V}\cdot\boldsymbol{n} &= 0 \\ \boldsymbol{n}\times(\boldsymbol{\tau}\cdot\boldsymbol{n}) &= 0 \end{aligned}\right\} \quad \text{for} \quad r = R, \tag{3b}$$

where $\boldsymbol{n}$ is the outward unit normal to the bubble surface. It is worth noting that the foregoing shear-free condition implies that the torque experienced by the bubble is always zero. This is why there is no reason to consider an eventual rotation of the bubble. The analytical results obtained in the low-Reynolds-number limit by Legendre & Magnaudet (1997) suggest that this conclusion would not be altered if the flow inside the bubble was taken into account: these authors considered a drop of arbitrary viscosity embedded in the flow field defined by (1) and showed that the matching of both tangential stresses and tangential velocities at the drop surface induces generally a non-zero rotation of the drop. However, the corresponding rotation rate was found to decrease from $\frac{1}{2}\alpha$ for a solid sphere to zero for an inviscid bubble. It seems thus reasonable to conclude that for a bubble the matching of the tangential velocities at the interface has a negligible influence on the outer flow whatever the Reynolds number.

Note that the situation regarding a possible rotation of the bubble would be dramatically different with a deforming bubble: in that case the torque experienced by a fixed bubble subjected to conditions (3*b*) would generally be non-zero and a freely moving bubble would rotate so as to maintain a zero torque. This rotation is probably the origin of the negative lift coefficient observed by several authors for highly deformed bubbles.

Under the above conditions the steady solution of the problem depends upon two characteristic parameters, namely the Reynolds number Re and the non-dimensional shear rate Sr, respectively defined by

$$Re = \frac{2RU_o}{\nu}, \quad Sr = \frac{2R\alpha}{U_o} \tag{4}$$

(in the remainder of the paper both U_o and α will be assumed to be positive). The latter quantity compares the streamwise velocity to the velocity difference induced by the shear over a distance corresponding to one bubble diameter. In the present work Re is varied between 0.1 and 500 and most of the computations concern two shear rates, namely $Sr = 0.02$ and $Sr = 0.2$. The latter value corresponds for example to a 1 mm diameter bubble rising at 20 cm s^{-1} in a shear of 40 s^{-1}, an order of magnitude typical of turbulent shear layers. Note that throughout this paper we consider a uniform shear flow extending to infinity in the y-direction. However, in many practical situations bubbles move into shear layers of finite thickness d_o. If d_o/R is large, both situations are certainly equivalent if the bubble Reynolds number is large (because the disturbance flow created by the bubble decreases like r^{-3}). The situation may be very different if Re is small because in that case the disturbance flow decreases like r^{-1} and the lift force results from weak inertia effects produced by the bubble in the far-field flow. This is why it would be interesting in the future to study the low-Reynolds-number motion of a bubble in a shear layer of finite thickness.

As stated in the introduction we are particularly interested in obtaining the lift and drag forces acting on the bubble, namely

$$F_L = \boldsymbol{e}_y \cdot \int_S \boldsymbol{\Sigma} \cdot \boldsymbol{n} \, \mathrm{d}S, \quad F_D = \boldsymbol{e}_x \cdot \int_S \boldsymbol{\Sigma} \cdot \boldsymbol{n} \, \mathrm{d}S, \tag{5}$$

where S denotes the surface of the bubble. The results concerning these forces will be expressed using the lift and drag coefficients C_L and C_D defined through the usual expressions

$$F_L \boldsymbol{e}_y = \rho \mathscr{V} C_L \boldsymbol{U} \times \boldsymbol{\omega}_o, \quad F_D \boldsymbol{e}_x = \tfrac{3}{8} \rho \frac{\mathscr{V}}{R} C_D |\boldsymbol{U}| \boldsymbol{U}, \tag{6}$$

where $\mathscr{V}$ is the bubble volume. In these expressions the unperturbed velocity $\boldsymbol{U}$ and the vorticity $\boldsymbol{\omega}_o = \boldsymbol{\nabla} \times \boldsymbol{U}$ must be evaluated at the centre of the bubble, leading to $\boldsymbol{U} = U_o \boldsymbol{e}_x$ and $\boldsymbol{\omega}_o = -\alpha \boldsymbol{e}_z$ in the present case.

As pointed out in the introduction, two analytical solutions giving the lift coefficient on a spherical bubble rising steadily in a simple shear flow have been derived so far. For an inviscid fluid satisfying the condition $Sr \quad 1$, Auton (1984, 1987) obtained the result

$$F_L = \tfrac{2}{3} \pi \rho R^3 \alpha U_o \tag{7a}$$

which yields the well-known lift coefficient

$$C_L = \tfrac{1}{2}. \tag{7b}$$

In the opposite limit of very viscous flows, Legendre & Magnaudet (1997) generalized the analysis performed by Saffman (1965) and McLaughlin (1991) for a solid sphere to

the case of a spherical drop with an arbitrary viscosity. For an inviscid bubble their result may be written

$$F_L = \frac{J(\varepsilon)}{\pi^2} R\left(\frac{\alpha}{\nu}\right)^{1/2} F^0 = \frac{4}{\pi}\rho\nu^{1/2}R^2 U_o\,\alpha^{1/2} J(\varepsilon). \tag{8a}$$

In this expression F^0 is the magnitude of the drag force on the bubble in creeping motion ($\boldsymbol{F}^0 = 4\pi\rho\nu R U_o\,\boldsymbol{e}_x$), ε is the dimensionless ratio defined by $\varepsilon = (Sr/Re)^{1/2}$ and $J(\varepsilon)$ is the value of a three-dimensional integral (McLaughlin 1991). The case $\varepsilon \to \infty$ corresponds to the high-shear-rate limit considered by Saffman and the corresponding value is $J(\infty) = 2.255$. Using (6) and (8*a*) one obtains the lift coefficient

$$C_L = \frac{6}{\pi^2}(Re\,Sr)^{-1/2} J(\varepsilon). \tag{8b}$$

The results (7*b*) and (8*b*) synthesize the present theoretical knowledge concerning the lift force produced on a spherical bubble by a simple shear flow. It must be stressed that both results have been derived under the assumption of a steady or nearly steady motion so that no theoretical information concerning possible transient effects affecting the lift force is available. In what follows all the computations start from the undisturbed flow field $\boldsymbol{V}(x, y, z, t = 0) = \boldsymbol{U}(y)$ and the transient stage will allow us to investigate some of these effects.

3. Numerical method

3.1. *Algorithm, grid system and boundary conditions*

The computations reported below have been carried out with the JADIM code developed in our group. This code solves the three-dimensional unsteady Navier–Stokes equations. The spatial discretization scheme used in JADIM has already been thoroughly described by Magnaudet *et al.* (1995) to which the reader is referred. Let us just mention that the momentum equations are written in velocity–pressure variables in a general system of orthogonal curvilinear coordinates. The discretization makes use of a staggered mesh and the equations are integrated in space using a finite volume method with second-order accuracy. The time-advancement algorithm used in the three-dimensional version of JADIM has been described by Calmet & Magnaudet (1997). Advective and viscous terms are computed through a second-order Runge–Kutta/Crank–Nicolson procedure while incompressibility is satisfied at the end of each time step by solving a Poisson equation for an auxiliary potential. In the present case we are mainly concerned with a steady solution which is obtained after several thousands of time steps when the maximum variation of the velocity field between two consecutive time steps becomes less than a certain value. However in §6 we will take advantage of the fact that the overall algorithm is second-order accurate in time to discuss the transient behaviour of the lift force.

A detail of the grid used in the present work is presented in figure 2. The three-dimensional orthogonal grid is obtained by rotating a two-dimensional grid around the axis $\boldsymbol{e}_x$ with an angle ϕ. The two-dimensional grid in the plane (x, y) is obtained by inverting the equations defining the streamlines $\psi = \text{const.}$ and the equipotential lines $\zeta = \text{const.}$ of the potential flow around a circle (see Magnaudet *et al.* 1995). Our previous studies (see e.g. Blanco & Magnaudet 1995) have shown that whatever the Reynolds number, no recirculation occurs behind a spherical clean bubble rising in a uniform flow. It seems thus reasonable to assume that no vortex shedding can occur for a spherical bubble moving in a linear shear flow, at least for moderate shears. Using

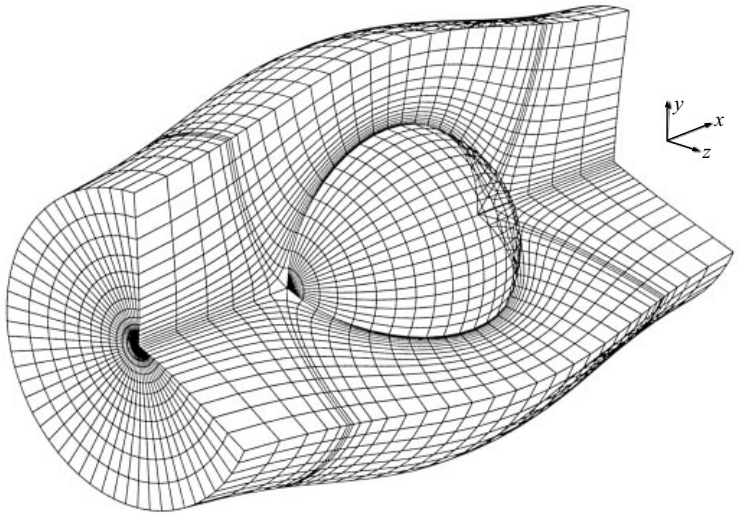

FIGURE 2. Partial view of the grid near the bubble.

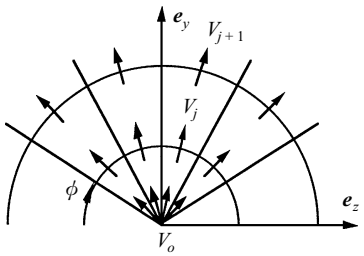

FIGURE 3. The grid in the vicinity of the x-axis.

this assumption we consider that the plane $z = 0$ is a symmetry plane for the present problem. Therefore, it is only necessary to solve the governing equations in a half-space, say $z \geqslant 0$.

Using this simplification, it appears that the computational domain is limited internally by a half-sphere corresponding to the bubble surface and externally by a half-cylinder. Several different boundary conditions are required on this outer boundary. The inflow velocity condition (3a) is imposed upstream, i.e. for a large negative value of x (this value will be specified later). A symmetry condition stating that both the normal velocity and the tangential stresses are zero is imposed on the plane $z = 0$. On the cylindrical boundary corresponding to large values of $(y^2+z^2)^{1/2}$ the boundary condition states that the normal velocity is zero and that the normal derivative of the tangential velocity corresponds to the unperturbed shear defined by (1), i.e. $\boldsymbol{V}\cdot\boldsymbol{n} = 0$ and $\boldsymbol{n}\cdot\boldsymbol{\nabla}[\boldsymbol{V}-(\boldsymbol{V}\cdot\boldsymbol{n})\boldsymbol{n}] = \alpha(\boldsymbol{e}_y\cdot\boldsymbol{n})\,\boldsymbol{e}_x$, $\boldsymbol{n}$ being the local unit normal to the boundary. Finally, a parabolic approximation of the governing equations allowing the flow to leave freely the domain without inducing significant perturbations is imposed downstream, i.e. for large positive values of x (see Magnaudet *et al.* 1995 for a detailed description). A specific condition is needed on the axis $\boldsymbol{e}_x$. This axis corresponds to the intersection of the N_ϕ planes $\phi = \text{const.}$ composing the grid. Thus for a given point $(x = x_o, y = 0, z = 0)$ one finds N_ϕ different values of the velocity V_o normal to the axis (figure 3). These N_ϕ values are not independent because they represent the projections on each plane $\phi = \text{const.}$ of the actual flow velocity at the point $(x = x_o, y = 0, z = 0)$. At first glance the values of V_o seem unimportant because no mass or momentum flux

crosses the $\boldsymbol{e}_x$-axis since the corresponding area is zero. However, these values are needed because they are involved in the expression for the normal viscous stresses on the staggered mesh. Several different boundary conditions were tested in order to obtain the best evaluation of these stresses (Legendre 1996). The best results were obtained by evaluating V_o through a second-order extrapolation of the neighbouring values V_j and V_{j+1} up to the axis (see figure 3).

The (ζ, ψ, ϕ)-grid used in the simulations reported below is made of $90 \times 45 \times 32$ nodes, the bubble surface being discretized with 22×32 nodes in the ζ- and ϕ-directions, respectively. A constant spacing is used along the azimuthal (ϕ) direction. In the ζ- and ψ-directions, i.e. in the (x, y)-plane, a geometrical progression ensuring that the ratio between two successive cells is less than 1.15 is chosen. In the immediate vicinity of the bubble surface, the thickness of the first rows of cells is about $0.01R$. This spacing allows us to locate four grid points within the boundary layer at the highest Reynolds number ($Re = 500$). This choice is satisfactory because it was shown by Blanco & Magnaudet (1995) that the present code captures properly viscous effects when this number of grid points lie in the boundary layer. Very close to the poles of the bubble the cells are larger owing to the singularity of the streamline $\psi = 0$ at these points. This implies that the boundary layer is less accurately described in these regions. This does not cause any serious problem of accuracy, especially in the evaluation of the hydrodynamic forces, because the axisymmetric character of the grid makes the contribution of the neighbourhood of the poles very small.

The computational domain extends to the same distance R_∞ upstream, downstream as well as in the direction normal to the $\boldsymbol{e}_x$-axis. Since the choice of R_∞ was found to be crucial for computing accurately the lift force, this point will be discussed in detail in the next subsection. A salient characteristic of the present computations is that, owing to the existence of the shear, the order of magnitude of the unperturbed velocity $\boldsymbol{U}$ may vary by more than one order of magnitude between the $\boldsymbol{e}_x$-axis and the outer boundary $(y^2+z^2)^{1/2} = R_\infty$. This fact has two consequences which explain why most of the computations reported below concern moderate shear rates. First, owing to the well-known CFL condition, the time step required to ensure the stability of the numerical algorithm is strongly reduced compared to usual situations where the velocity keeps a constant order of magnitude throughout the computational domain. Secondly, the unperturbed velocity is negative for $y_o < -U_o/\alpha$. Thus when the shear increases, the streamwise velocities become necessarily negative for large negative values of y. This leads to numerical difficulties because the role of the inlet and outlet boundaries is reversed in these regions of the flow. More precisely if the outflow boundary conditions are imposed everywhere on the boundary $x = +R_\infty$ without taking into account the actual direction of the local flow, numerical perturbations can be introduced in the computational domain and can contaminate the flow field, especially if the Reynolds number is large. To avoid this problem, in most of the high-shear-rate computations reported in §7 the boundary condition imposed in the plane $x = +R_\infty$ is modified as follows. The usual parabolic outflow condition is imposed at all points of the boundary belonging to the disk $(y^2+z^2)^{1/2} < U_o/\alpha$ (where the unperturbed velocity is positive) while the inflow condition $\boldsymbol{V} = \boldsymbol{U}$ is imposed in the ring $U_o/\alpha < (y^2+z^2)^{1/2} < R_\infty$. This mixed condition enables the far wake to leave the computational domain while preventing numerical perturbations being generated by the negative velocities.

Near the bubble the grid lines shown in figure 2 are highly curved. Thus the curvilinear source terms involved in the momentum equations (see Magnaudet *et al.* (1995) have a significant weight in that crucial region. It is obviously very important

to evaluate correctly these terms and more precisely the curvature radii that they involve. To reach this goal, Legendre (1996) developed a procedure allowing us to ensure that these curvilinear terms cannot create artificial sinks or sources of momentum in the discrete equations. Basically what must be enforced in the momentum equations are the fundamental properties of constant vectors and tensors expressed in a discrete sense. For example one must ensure that the discrete value of the divergence of any constant tensor $\boldsymbol{T}$ built on the vectors $\boldsymbol{e}_x$, $\boldsymbol{e}_y$ and $\boldsymbol{e}_z$ (for example $\boldsymbol{T} = \boldsymbol{e}_x \boldsymbol{e}_y$) is zero everywhere. Using the expression for the divergence of a second-order tensor in curvilinear orthogonal coordinates, the foregoing requirement can be written under the form of three equations, one along each local coordinate line. Then these equations can be put in finite volume form and can be discretized exactly with the same spatial schemes as those used for solving the momentum equations. Knowing the local value of each component of the constant tensor $\boldsymbol{T}$, one obtains three relations between the radii of curvature. A linear system is then formed and solved in order to determine the local value of the radii of curvature which will finally be used in the momentum equations.

3.2. *Preliminary testing*

The JADIM code has been extensively used in the past, especially for axisymmetric flows around bubbles and rigid particles (see Magnaudet *et al.* 1995; Blanco & Magnaudet 1995; Cuenot *et al.* 1997) or for three-dimensional turbulent flows (Calmet & Magnaudet 1997). Consequently only tests related to the geometrical or physical specificities of the present problem are required to ensure that the computational results are correct.

A first series of tests was carried out in order to determine the optimal size R_∞ of the computational domain. Five domains extending up to $R_\infty/R = 20$, 40, 60, 80 and 100, respectively, were used at both low and high Reynolds number ($Re = 0.1$, 1, 500) for a non-dimensional shear rate $Sr = 0.02$. The drag and lift coefficients obtained in these simulations are reported in table 1. At high Reynolds number, it is clear that a domain extending up to 20 radii is sufficient because no modification is noticed either to the drag force or to the lift force when the size of the domain is increased. In contrast, for the low-Reynolds-number cases it appears that confinement effects have a tremendous influence on the lift force. The results obtained for $Re = 0.1$ show that, for the present value of Sr, even a domain extending up to 100 radii is not sufficient to capture properly all the inertia effects responsible for the lift force. This conclusion is not very surprising: the theoretical analysis leading to (8*a*) shows that the inertia and viscous effects induced by the bubble become comparable at a distance $R_S/R = O(2(Re\,Sr)^{-1/2})$. In the present case one gets $R_S/R \approx 45$, a result suggesting that $R_\infty/R = 100$ is not sufficient. Based on these tests, the computation domain chosen for almost all the simulations extends up to 80 radii when $Re > 0.2$. To save computational resources, the size of the domain was only increased up to 100 radii for $Re = 0.1$ and 0.2. Thus, as already pointed out, the results obtained for the lift force at $Re = 0.1$ and $Sr = 0.02$ are certainly not very accurate. No computation was carried out at Reynolds numbers lower than 0.1 because of the foregoing limitation and also because our main interest in the low-Reynolds-number limit was to determine the bounds of validity of the asymptotic solution (8*b*), a goal which can be reached by exploring the range $0.1 \leqslant Re \leqslant 1$.

A second series of simulations was carried out in order to check the numerical condition imposed on the axis $\boldsymbol{e}_x$. The first test consisted in computing the flow induced around the bubble by the undisturbed flow $\boldsymbol{U} = (U_o + \alpha y)\,\boldsymbol{e}_x$ parallel to $\boldsymbol{e}_x$ (Case 1) and by the undisturbed flow $\boldsymbol{U} = (U_o + \alpha x)\,\boldsymbol{e}_y$ orthogonal to $\boldsymbol{e}_x$ (Case 2). Then the drag and

		20 radii	40 radii	60 radii	80 radii	100 radii
$Re = 0.1$	C_D	172.2	162.2	163.3	162.5	162.1
	C_L	2.87	5.01	6.57	7.52	7.97
$Re = 1$	C_D	17.88	17.52	17.49	17.47	17.46
	C_L	0.997	0.631	0.486	0.421	0.419
$Re = 500$	C_D	0.0890	0.0890	0.0889	0.0889	0.0889
	C_L	0.489	0.489	0.488	0.488	0.488

TABLE 1. Effect of the size of the computational domain on the drag and lift coefficients ($Sr = 0.02$)

	Case 1 $\boldsymbol{U} = (U_o + \alpha y)\,\boldsymbol{e}_x$	Case 2 $\boldsymbol{U} = (U_o + \alpha x)\,\boldsymbol{e}_y$	Difference (%)
C_D	0.0889	0.0886	0.3
C_L	0.488	0.490	0.4

TABLE 2. Comparison between the lift and drag coefficients found for the unperturbed flows $\boldsymbol{U} = (U_o + \alpha y)\,\boldsymbol{e}_x$ and $\boldsymbol{U} = (U_o + \alpha x)\,\boldsymbol{e}_y$ at $Re = 500$

		C_D		C_L		C_Ω	
Re_∞	Re_Ω	Num.	Anal.	Num.	Anal.	Num.	Anal.
0	0.4	—	—	—	—	160.5	160
0.1	0.4	247.1	244.5	0.371	0.375	161.1	160

TABLE 3. Torque, lift and drag coefficients on a rotating solid sphere moving in a uniform flow ($Re_\Omega = 0.1$). Comparison with the analytical results of Lamb (1932) and Rubinow & Keller (1961)

lift forces calculated in these two configurations were compared. In Case 2 the primary flow had to cross the $\boldsymbol{e}_x$-axis while in Case 1 only the secondary velocities had to cross this singular axis. This comparison was thus relevant for estimating the performance of the numerical treatment of the singularity on the axis $\boldsymbol{e}_x$. The results obtained in both configurations at $Re = 500$ for $Sr = 0.02$ are reported in table 2). The difference is less than 1% for both the drag and the lift coefficients. To confirm this positive conclusion another test was performed at low Reynolds number. It consisted in computing the flow around a solid sphere rotating with the angular velocity Ω around the $\boldsymbol{e}_z$-axis (the shear-free bubble could not be used for that purpose because its rotation does not induce any motion in the liquid). This test is also interesting because the main flow must cross the $\boldsymbol{e}_x$-axis on both sides of the sphere. When no mean flow exists, the well-known solution of the Stokes equation (see Lamb 1932, p. 589) leads only to a torque with an associated moment coefficient C_Ω equal to $64/Re_\Omega$ (with $Re_\Omega = (2R)^2\Omega/\nu$). In contrast when the sphere moves with a velocity U_∞, a drag and a lift force appear (Rubinow & Keller 1961). For low Reynolds numbers the drag coefficient is identical to the one provided by Oseen's solution (see Lamb 1932, p. 617), i.e. $C_D = 24/Re_\infty + 9/2$ (with $Re_\infty = 2RU_\infty/\nu$) and the moment coefficient is unchanged. Rubinow & Keller found that in this flow regime the lift coefficient C_L defined through (6) was at first order $C_L = 3/8$. The numerical tests were performed at $Re_\Omega = 0.4$ for both $Re_\infty = 0$ and 0.1. The results of these tests are reported in table 3. The difference

between the numerical prediction and the analytical solution never exceeds 1.5%. This result is very satisfactory since it was obtained with a grid which is not very well adapted to the flow under consideration. When a polar grid is used, the streamlines are parallel to the grid lines and much more accurate results are obtained (Legendre 1996). The two foregoing tests allow us to conclude that, whatever the Reynolds number the condition imposed on the singular axis $\boldsymbol{e}_x$ disturbs the flow only very slightly, even when the streamlines of the main flow have to cross this axis.

4. The flow field

Having established the ability of the numerical code to compute asymmetric flows around a sphere, we turn now to explore the characteristics of the shear flow around the bubble. Figures 4 and 5 show the disturbance velocity field $\boldsymbol{v} = \boldsymbol{V} - \boldsymbol{U}$ in the symmetry plane $z = 0$ for various flow conditions. The general structure corresponding to a uniform flow ($Sr = 0$) and the Reynolds number effects can be easily recognized. At high Reynolds number (figure 4*a–c*), the disturbance flow increases rapidly with the distance to the bubble, except in the thin wake which is clearly present downstream of the bubble. In contrast at low Reynolds number (figure 5) the disturbance flow remains significant at larger distances from the bubble and preserves the fore-and-aft symmetry with respect to the bubble. When the shear rate is weak (figure 4*a*), the flow field is almost symmetric about the $\boldsymbol{e}_x$-axis. Then, when the shear rate increases and the Reynolds number is high, the difference between the upper half-plane $\phi = 0$ and the lower one $\phi = \pi$ becomes more and more prominent (figures 4*b* and 4*c*). At the highest shear rate (figure 4*c*), the wake is very short and has an unusual structure: its thickness seems to decrease quickly with the distance to the bubble and its mean direction is deflected towards the upper half-plane suggesting suction by the lower pressures found in that part of the flow. Downstream of the bubble the structure of the disturbance flow is completely dominated by the role of the shear: the y-component of the velocity is negative everywhere, meaning that the symmetry with respect to the plane $y = 0$ is not recovered at such distances. Comparing figures 4(*b*) and 5 clearly demonstrates that for a given shear rate the asymmetry increases with the Reynolds number: for $Re = 1$, the flow looks nearly symmetric while the deflection of the wake is obvious for $Re = 500$.

Another interesting view of the flow structure is provided by figures 6 and 7, which show the streamwise component of the vorticity, ω_x (normalized by the shear α), in the equatorial plane $x = 0$ (figure 6) and in the plane $x/R = 2$ located one radius downstream of the bubble (figure 7). This vorticity component, called 'trailing vorticity' by Lighthill (1956) is a central ingredient of the shear flow around a sphere: it is zero in the primary flow defined by (1) as well as in the boundary layer and the wake of a sphere embedded in an axisymmetric flow. It results basically from the tilting and stretching of the primary vorticity $-\alpha\boldsymbol{e}_z$ by the spanwise velocity gradient $\partial(\boldsymbol{V}\cdot\boldsymbol{e}_x)/\partial z$ induced by the presence of the sphere. The asymptotic analysis of Lighthill (1956) and Auton (1984, 1987) predicts that ω_x is a linear function of $\sin\phi$. This implies that in the limit $Sr \to 0$, ω_x must be symmetric with respect to the plane $y = 0$. Figures 6 and 7 show that this is still approximately true for $Sr = 0.2$. However, nonlinear effects due to the finite value of Sr produce slightly larger values of ω_x in the lower half of the flow. Figure 6 illustrates the influence of viscous effects on the spatial structure of the ω_x distribution close to the bubble: while ω_x is negative (for $z > 0$) at $Re = 50$ (figure 6*a*), an outer region of positive values appears at $Re = 100$ (figure 6*b*). For larger values of Re (figures 6*c* and 6*d*) the negative values have completely disappeared. This evolution is related to that of the azimuthal velocity V_ϕ described

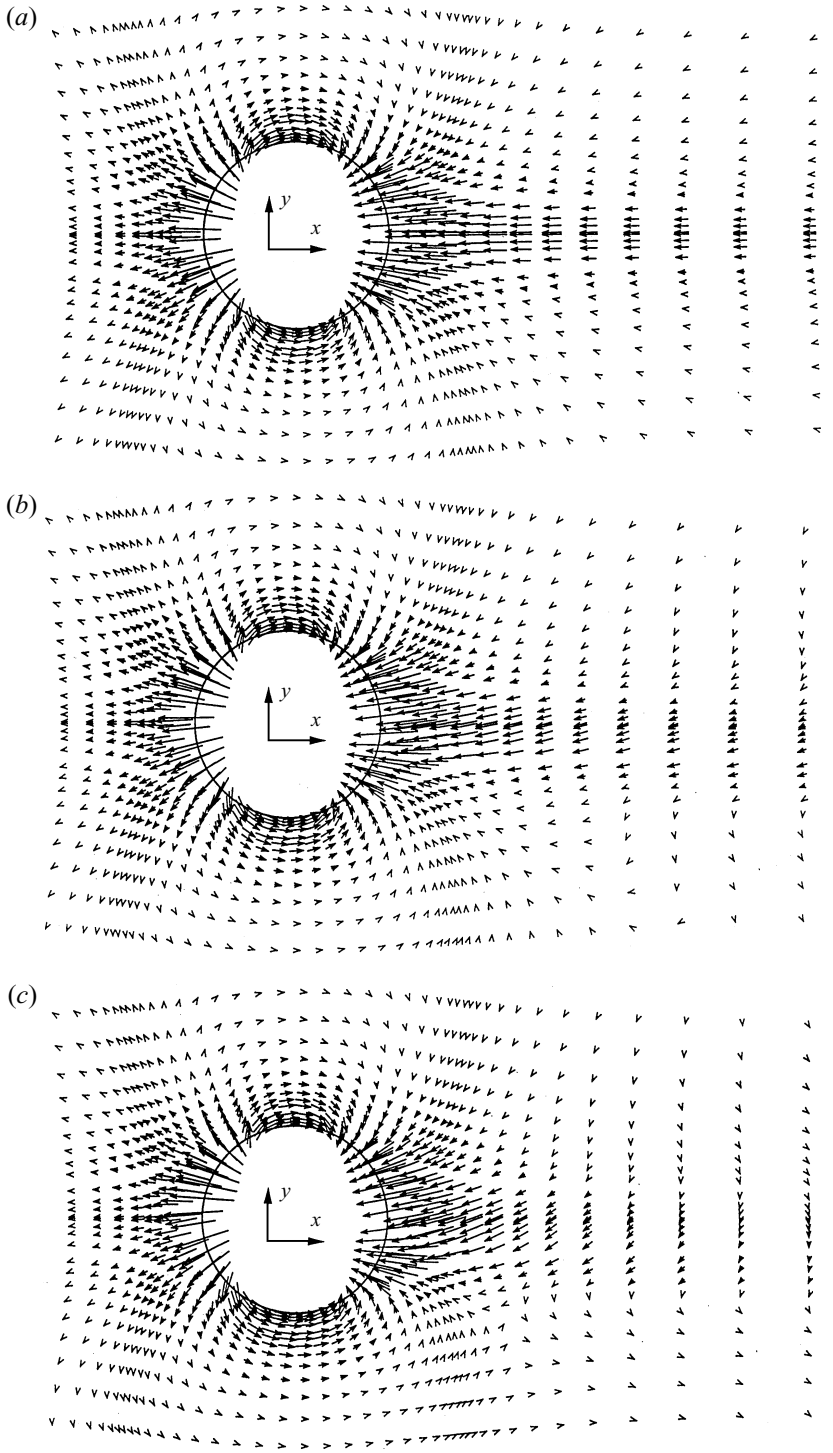

FIGURE 4. Disturbance velocity field $\boldsymbol{v} = \boldsymbol{V} - \boldsymbol{U}$ in the plane $(\boldsymbol{e}_x, \boldsymbol{e}_y)$ for $Re = 500$. (*a*) $Sr = 0.02$; (*b*) $Sr = 0.2$; (*c*) $Sr = 0.4$.

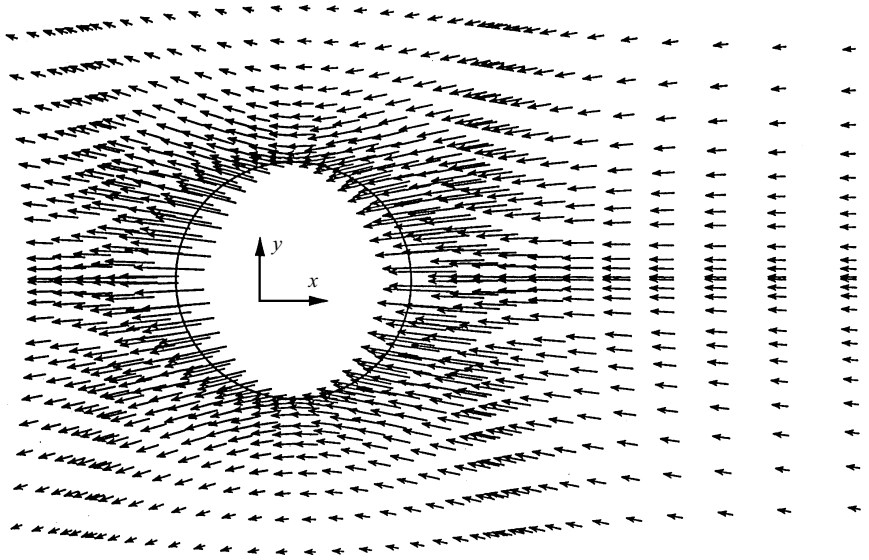

FIGURE 5. Disturbance velocity field $\boldsymbol{v} = \boldsymbol{V} - \boldsymbol{U}$ in the plane $(\boldsymbol{e}_x, \boldsymbol{e}_y)$ for $Re = 1$ and $Sr = 0.2$.

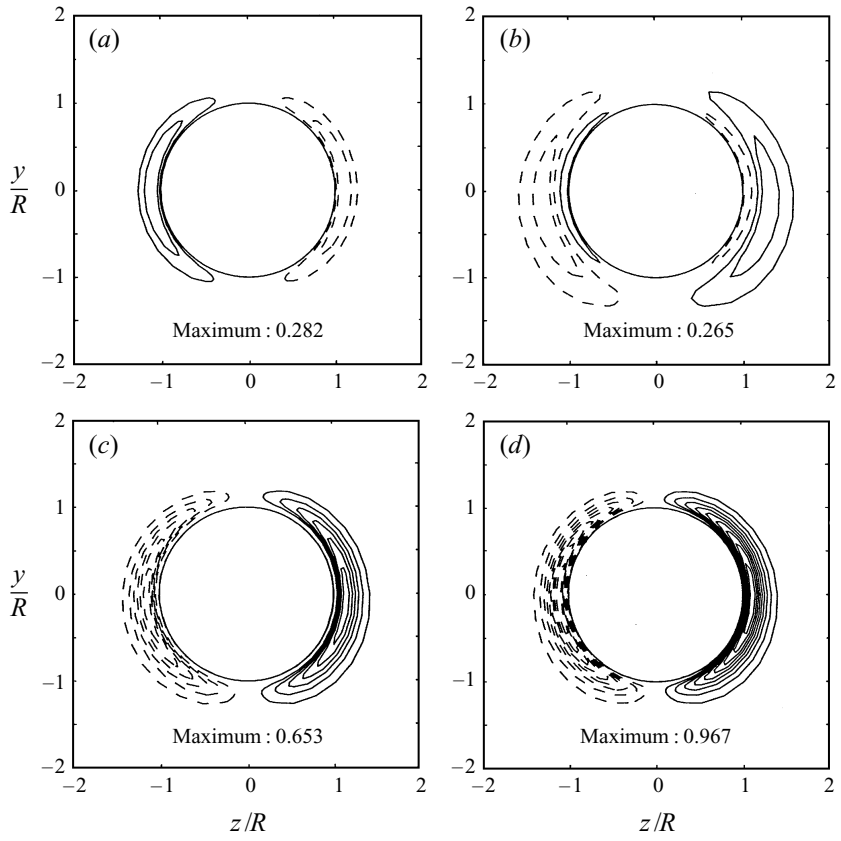

FIGURE 6. Iso-values of the streamwise vorticity ω_x (normalized by α) in the equatorial plane $x/R = 0$. (*a*) $Re = 50$; (*b*) $Re = 100$; (*c*) $Re = 300$; (*d*) $Re = 500$; ——, positive values; -----, negative values (the increment between two consecutive iso-values is $\Delta\omega_x = 0.1$).

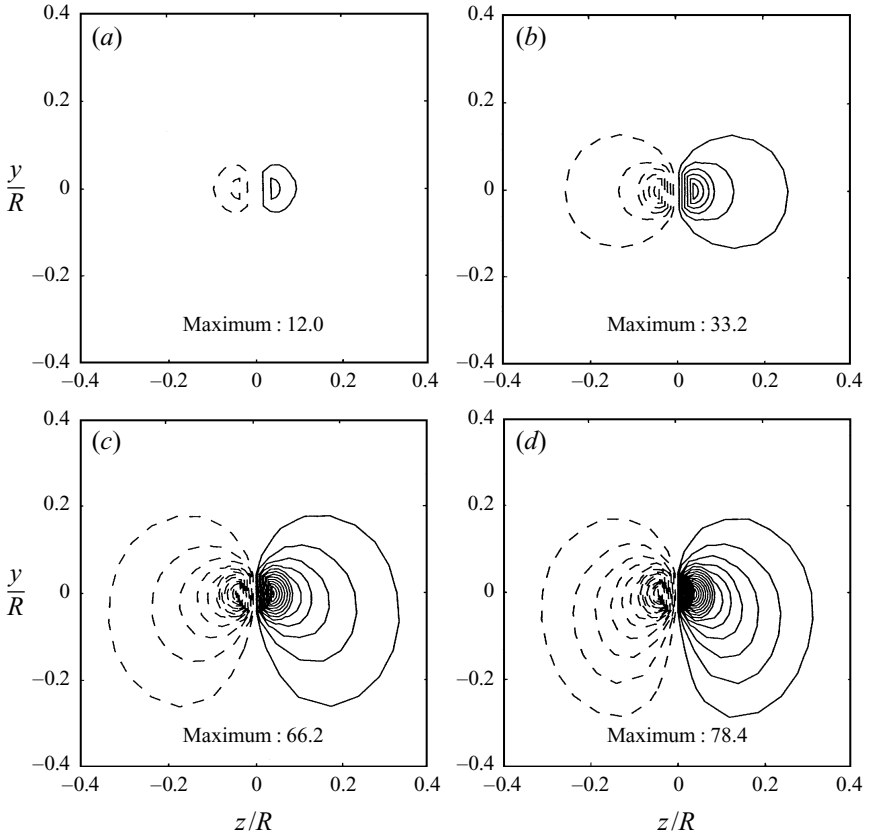

FIGURE 7. As figure 6 but in the plane $x/R = 2$ (the increment between consecutive iso-values is $\Delta\omega_x = 5$).

below. It shows that for $z > 0$, the velocity gradients induced by viscous effects tend to produce negative values of ω_x while the velocity gradients resulting from the inviscid vortex stretching mechanism generate positive values of ω_x. At the highest Reynolds number, figure 6(*d*) indicates that the maximum value of ω_x is of the same order of magnitude as the unperturbed shear. Nevertheless, this value cannot be compared with those obtained in the inviscid limit by Lighthill and Auton because very close to the bubble viscous effects are always significant. In contrast, such a comparison can be carried out far enough from the bubble. For example the values tabulated by Auton yield $\omega_x(x/R = y/R = 0,\ z/R = 1.32) = 0.243$ while present results obtained at $Re = 500$ yield $\omega_x = 0.215$.

Figure 7 shows that, downstream of the bubble, the significant values of ω_x are concentrated within two thin vortex tubes whose centres are located very close to the x-axis. The effect of the Reynolds number is also clearly apparent in this figure. At low to moderate Reynolds number, say for $Re \leqslant 100$ (figures 7*a* and 7*b*), the maximum of ω_x is small because viscous effects quickly diffuse the trailing vorticity once it has been produced around the sphere. This maximum increases very strongly with Re and reaches values which are about two orders of magnitude larger than the primary vorticity for the highest Reynolds numbers considered here (figures 7*c* and 7*d*). As previously, these maxima cannot be compared with those predicted by the inviscid theory because of the presence of viscous effects in the central region of the wake. In

contrast this comparison is legitimate in the outer region. Using the discrete values tabulated by Auton yields for example $\omega_x(x/R = 2, y/R = 0, z/R \approx 0.35) \approx 3.05$ while the corresponding value in figure 7*d*) is 3.30. The two quantitative comparisons reported above suggest that for $Re = 500$, present values of ω_x found in the nearly inviscid regions of the flow are in good agreement with those predicted by the inviscid theory, the small differences being probably due to small nonlinear effects related to the finite value of Sr. It must be noted that further downstream ω_x keeps significant values for high enough Reynolds numbers because the disturbance produced by the bubble is slowly dissipated by viscosity. For example the numerical results indicate that for $Re = 500$ and $Sr = 0.2$ the maximum of ω_x at $x/R = 25$ is still about 1.3, while it is about 0.1 for $x/R = 50$. These values show that the trailing vorticity still has the same order of magnitude as the imposed shear at downstream distances larger than ten bubble diameters.

In view of the discussion on the hydrodynamic forces, a detailed description of the distribution of the tangential velocity at the surface of the bubble is also in order. Actually the tangential velocity has two components, namely one meridian component $V_\theta(\theta, \phi) = \boldsymbol{V}(r = R, \theta, \phi)\cdot\boldsymbol{e}_\theta$ lying in the plane $\phi = $ const. and one azimuthal component $V_\phi(\theta, \phi) = \boldsymbol{V}(r = R, \theta, \phi)\cdot\boldsymbol{e}_\phi$ lying in the plane $\theta = $ const. normal to the unperturbed flow (see figure 1 for the definition of the local axes). Indeed, V_ϕ is a crucial quantity for the present problem since the lift force results directly from the fact that the pressure and the normal viscous stresses have a non-constant azimuthal distribution. Taking into account the kinematic boundary condition at the bubble surface, the governing equation for V_ϕ may be written (Batchelor 1967, p. 601)

$$\boldsymbol{V}\cdot\boldsymbol{\nabla}V_\phi + \frac{\operatorname{cotan}\theta}{R}V_\theta V_\phi = -\frac{1}{\rho R\sin\theta}\frac{\partial P}{\partial\phi} + \nu\nabla^2 V_\phi + \frac{\nu}{R^2\sin^2\theta}\left[2\cos\theta\frac{\partial V_\theta}{\partial\phi} - V_\phi\right]. \qquad (9)$$

Since $\boldsymbol{U}\cdot\boldsymbol{e}_\phi = 0$, V_ϕ vanishes far from the bubble, i.e. V_ϕ is a secondary velocity which does not directly result from the unperturbed flow. From (9) it is straightforward to see how V_ϕ is produced at low Reynolds number: owing to the shear α, the meridian velocity $V_\theta(\theta, \phi = 0)$ at the top of the bubble is larger than its counterpart $V_\theta(\theta, \phi = \pi)$ at the bottom. The viscous term of (9) involving $\partial V_\theta/\partial\phi$ is thus non-zero and the balance between the various terms induces non-zero values of V_ϕ and $\partial P/\partial\phi$ (however it must be noted that in the creeping flow limit V_ϕ remains zero because $\partial P/\partial\phi$ balances exactly the term proportional to $\partial V_\theta/\partial\phi$). In contrast, in the high-Reynolds-number limit no source term exists in (9). Under such conditions the origin of V_ϕ must be sought in the balance equation determining the pressure field: taking the divergence of (2*b*) one gets

$$-\frac{1}{\rho}\nabla^2 P = \boldsymbol{\nabla}\cdot(\boldsymbol{V}\cdot\boldsymbol{\nabla}\boldsymbol{V}). \qquad (10)$$

Since the right-hand side of (10) involves terms like V_θ and $\partial V_\theta/\partial\theta$ which depend on ϕ, the pressure field is necessarily non-uniform along the azimuthal direction, i.e. a pressure gradient $\partial P/\partial\phi$ appears. Then (9) shows that V_ϕ results from a balance between the advective terms and this azimuthal pressure gradient. Since no azimuthal velocity exists when $Sr = 0$, V_ϕ scales necessarily with $R\alpha$. Consequently V_ϕ is generally several orders of magnitude smaller than V_θ whose maximum lies in the range $[\frac{1}{2}U_o, \frac{3}{2}U_o]$ when $Sr = 0$ (see Magnaudet *et al.* 1995). For that reason it is more convenient to study the tangential velocity field at the bubble surface using the decomposition

$$\boldsymbol{V}(r = R, \theta, \phi) = U_o\,\boldsymbol{V}_U(\theta) + R\alpha\tilde{\boldsymbol{v}}(\theta, \phi), \qquad (11)$$

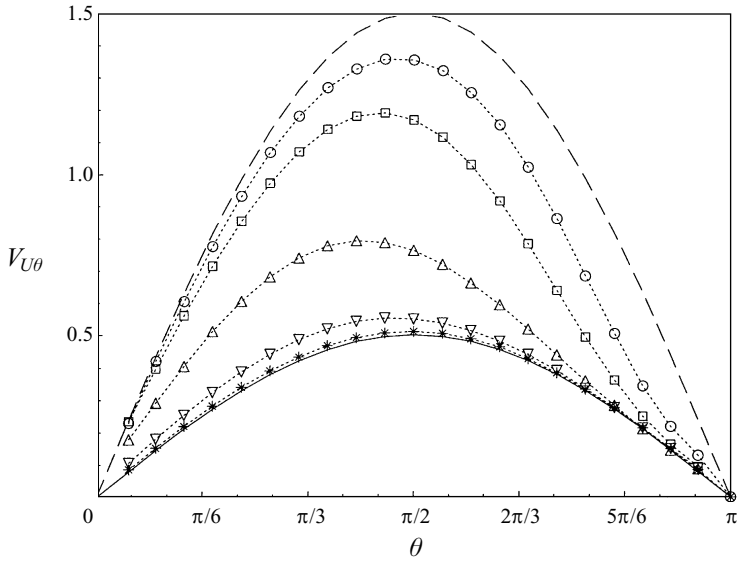

FIGURE 8. Meridian velocity $V_{U\theta}(\theta)$ corresponding to $Sr = 0$. ——, potential solution; ——, Stokes solution; ·····, numerical results: ○, $Re = 500$; □, $Re = 100$; △, $Re = 10$; ▽, $Re = 1$; *, $Re = 0.1$.

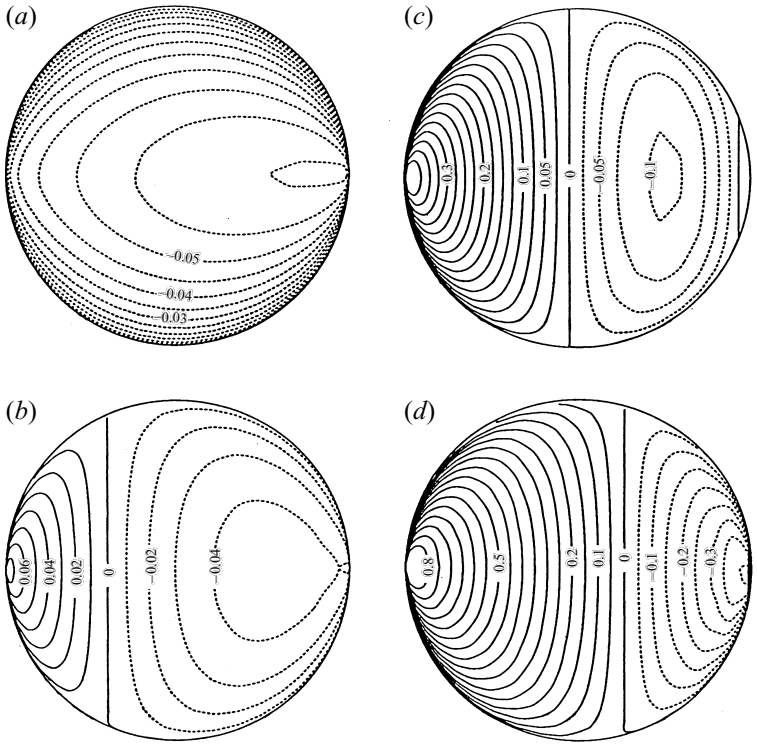

FIGURE 9. Surface iso-contours of the azimuthal velocity $\tilde{v}_\phi(\theta, \phi)$ for $Sr = 0.02$: (*a*) $Re = 0.1$; (*b*) $Re = 1$; (*c*) $Re = 10$; (*d*) $Re = 500$; ——, positive values; ·····, negative values. The flow is from left to right and the positive velocities are directed towards the bottom of the bubble.

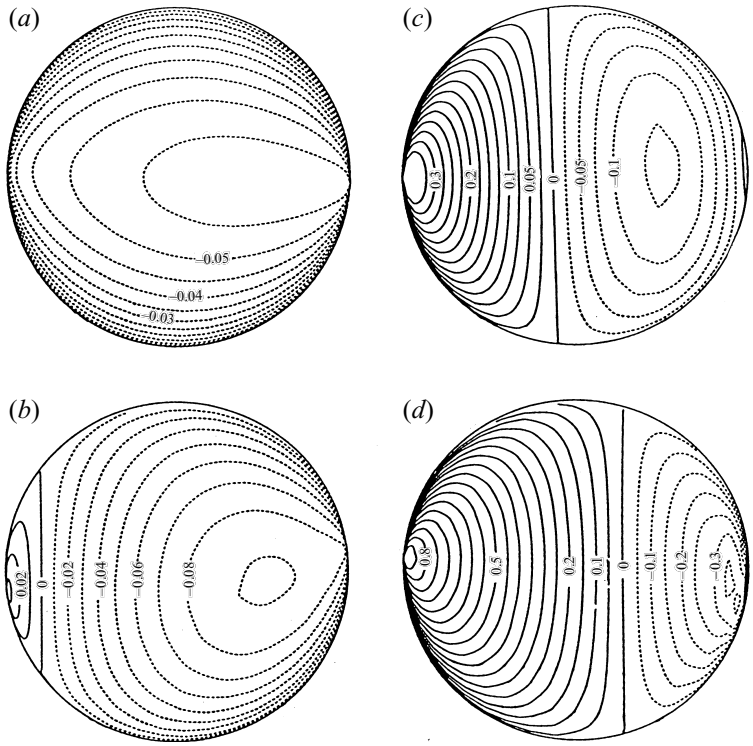

FIGURE 10. As figure 9 but for $Sr = 0.2$.

where $\boldsymbol{V}_U(\theta) = V_{U\theta}(\theta)\,\boldsymbol{e}_\theta$ is the non-dimensional velocity at the surface of the bubble corresponding to the axisymmetric situation $Sr = 0$, and $\tilde{\boldsymbol{v}}$ is the non-dimensional velocity resulting from the presence of the shear. The meridian velocity $V_{U\theta}(\theta)$ obtained by solving the axisymmetric flow around the bubble at several different Reynolds numbers in the range $0.1 < Re < 500$ is plotted in figure 8. One sees in that figure that, whatever the Reynolds number, $V_{U\theta}$ has a nearly symmetric distribution with respect to the equatorial plane $\theta = \frac{1}{2}\pi$ and that a significant difference exists between the actual distribution and the potential solution even for $Re = 500$. The iso-values of the azimuthal component $\tilde{v}_\phi(\theta, \phi)$ are plotted in figures 9 and 10 for $Sr = 0.02$ and $Sr = 0.2$ and for several values of the Reynolds number. It is clear in these figures that the Reynolds number has a major influence on both the intensity and the sign of $\tilde{v}_\phi$. At low Reynolds number $\tilde{v}_\phi$ is negative everywhere, i.e. the azimuthal velocity is uniformly directed towards the top of the bubble. Then when the Reynolds number increases, the momentum diffusion in the azimuthal direction decreases, resulting in a progressive change in the sign of $\tilde{v}_\phi$ starting at the upstream part of the bubble. For $Re = 500$, $\tilde{v}_\phi$ is positive over nearly two thirds of the bubble. However, the influence of the viscosity is still significant at that Reynolds number because Auton's (1984, 1987) calculation predicts positive values of $\tilde{v}_\phi$ everywhere on the surface for an inviscid flow. The magnitude of $\tilde{v}_\phi$ is also greatly affected by the Reynolds number: at $Re = 500$ the maximum of $\tilde{v}_\phi$ is about 0.9 while the maximum negative value found at $Re = 0.1$ is about -0.06. Finally, comparison of figures 9 and 10 also shows that the distribution of $\tilde{v}_\phi$ is affected by the magnitude of Sr when the Reynolds number is moderate. This is especially the case for $Re = 1$ where $\tilde{v}_\phi$ is positive over a much larger part of the bubble when $Sr = 0.02$ than when $Sr = 0.2$.

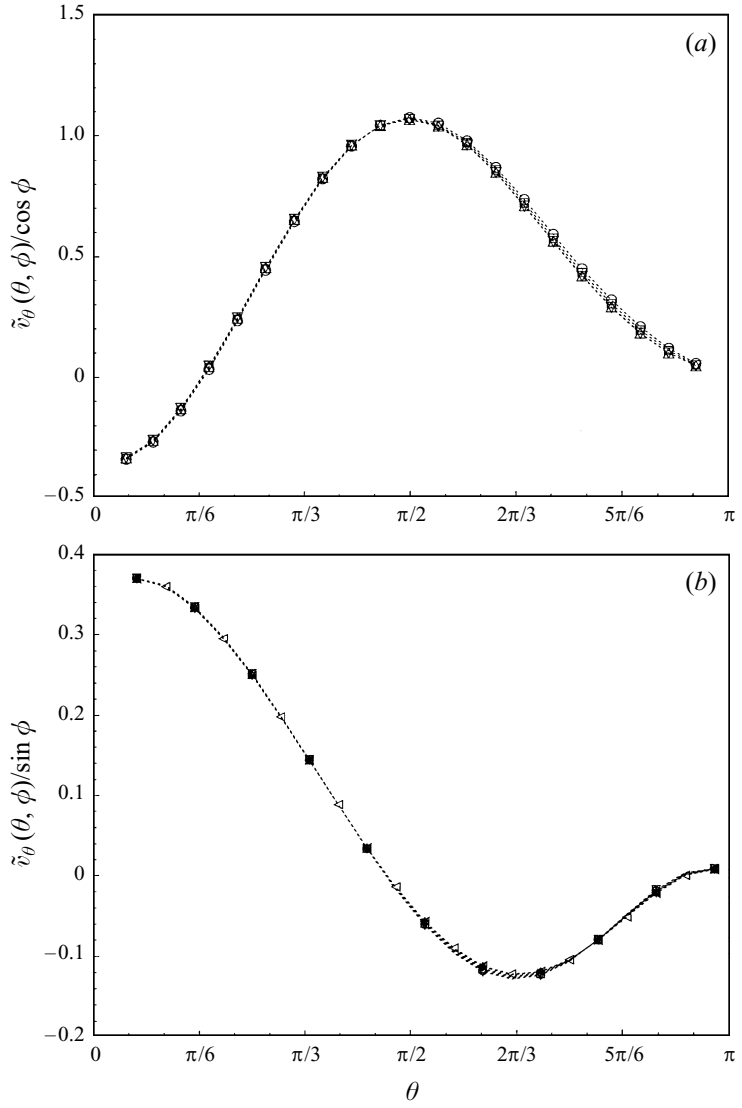

FIGURE 11. Distribution of (*a*) the meridian velocity $\tilde{v}_\theta(\theta,\phi)/\cos\phi$ ($\bigcirc$, $\phi=0$; $\square$, $\phi=\frac{1}{4}\pi$; $\triangle$, $\phi=\frac{3}{4}\pi$; $\triangledown$, $\phi=\pi$) and (*b*) the azimuthal velocity $\tilde{v}_\phi(\theta,\phi)/\sin\phi$ ($\bigcirc$, $\phi=0$; $\square$, $\phi=\frac{1}{4}\pi$; $\triangle$, $\phi=\frac{3}{8}\pi$; $\triangledown$, $\phi=\frac{1}{2}\pi$; $\diamond$, $\phi=\frac{5}{8}\pi$; *, $\phi=\frac{3}{4}\pi$; $\triangleleft$, $\phi=\frac{7}{8}\pi$), for $Re=10$ and $Sr=0.2$.

For $Sr=0.02$, the plot of the numerical results (not shown here) reveals that for $Re\geqslant 5$, $\tilde{\boldsymbol{v}}$ follows the spatial distribution found by Lighthill (1956) for an inviscid flow and a small shear rate, namely

$$\tilde{\boldsymbol{v}}\cdot\boldsymbol{e}_\theta=\tilde{v}_\theta(\theta,\phi=0)\cos\phi,\quad \tilde{\boldsymbol{v}}\cdot\boldsymbol{e}_\phi=\tilde{v}_\phi(\theta,\phi=\tfrac{1}{2}\pi)\sin\phi. \tag{12a,b}$$

The same behaviour is also observed for $Sr=0.2$ in a similar range of Re. For $Re=10$ (figure 11*a*,*b*) the results follow the foregoing distribution extremely well. The same is true at $Re=1$ for the meridian velocity (figure 12*a*) but not for the azimuthal velocity since figure 12(*b*) reveals a more complex dependence on ϕ. It will be shown later that this behaviour seems to correspond to the transition between the regime dominated by viscous diffusion and the inertial regime. The distributions (12*a*,*b*) result

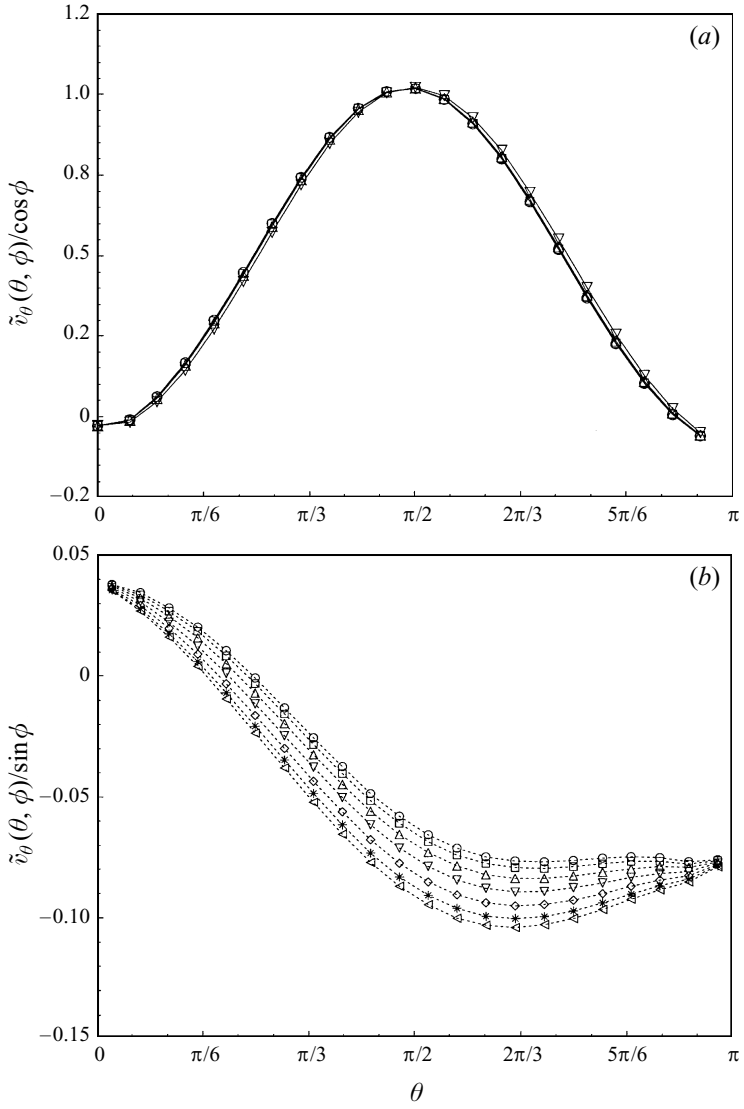

FIGURE 12. As figure 11 but for $Re = 1$.

from spatial symmetries of the vorticity field. Therefore the behaviour displayed in Figure 11 shows that the vorticity field retains the same spatial structure at Reynolds numbers of a few units as that in inviscid flow.

The tangential components $\tilde{v}_\theta(\theta, \phi = 0)$ and $\tilde{v}_\phi(\theta, \phi = \frac{1}{2}\pi)$ corresponding to $Sr = 0.02$ are plotted in figures 13 and 14 for different Reynolds numbers. They are compared with the tangential velocities calculated in inviscid fluid by Auton (1984, 1987) and with those derived from the creeping flow solution, namely

$$\tilde{\boldsymbol{v}}_\theta^{\mathrm{St}} = \sin^2\theta\cos\phi \quad \text{and} \quad \tilde{\boldsymbol{v}}_\phi^{\mathrm{St}} = 0. \tag{13a}$$

As expected, the Reynolds number has a tremendous effect on both tangential velocities, and the comparison between numerical results and Auton's calculation shows that viscous effects remain significant even for $Re = 500$. This result is not

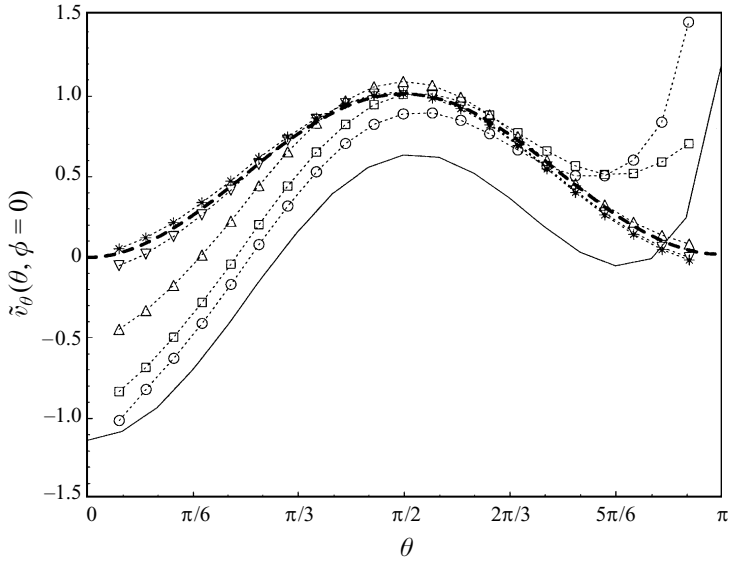

FIGURE 13. Evolution of the meridian velocity $\tilde{v}_\theta(\theta, \phi = 0)$ with the Reynolds number ($Sr = 0.02$). - - - - -, Stokes solution (13*a*); ——, Auton (1984, 1987); ·····, numerical results: ○, $Re = 500$; □, $Re = 100$; △, $Re = 10$; ▽, $Re = 1$; *, $Re = 0.1$.

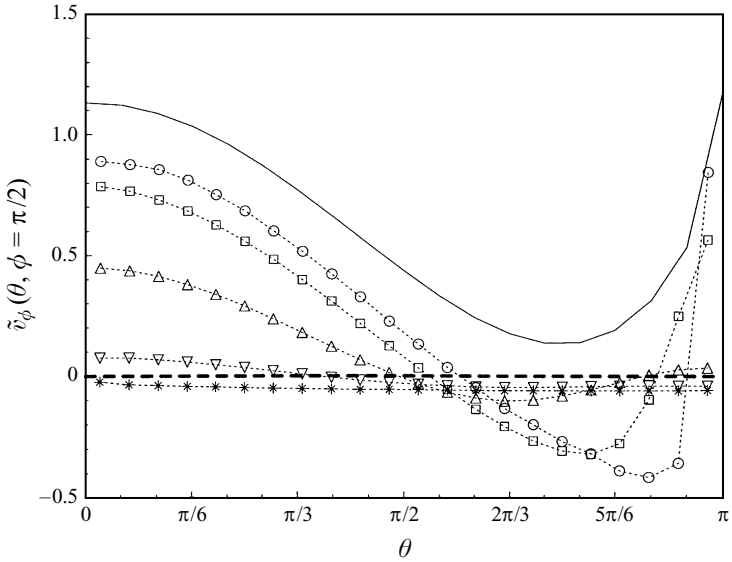

FIGURE 14. As figure 13 but for the azimuthal velocity $\tilde{v}_\phi(\theta, \phi = \frac{1}{2}\pi)$.

surprising since it was already shown in figure 8 that at this Reynolds number the primary meridian velocity $V_{U\theta}(\theta)$ is about 10% lower than the potential solution $V_{U\theta}(\theta) = \frac{3}{2}\sin\theta$ used in Auton's theory. In contrast the secondary velocity $\tilde{v}_\theta(\theta, 0)$ is found to be higher by about 10% than Auton's prediction (see figure 13). This increase is certainly due to the vorticity generated at the bubble surface by the shear-free condition; this vorticity is not taken into account in the inviscid theory of Auton but it may well contribute to increase the production of $\tilde{v}_\theta$ (this could be checked by

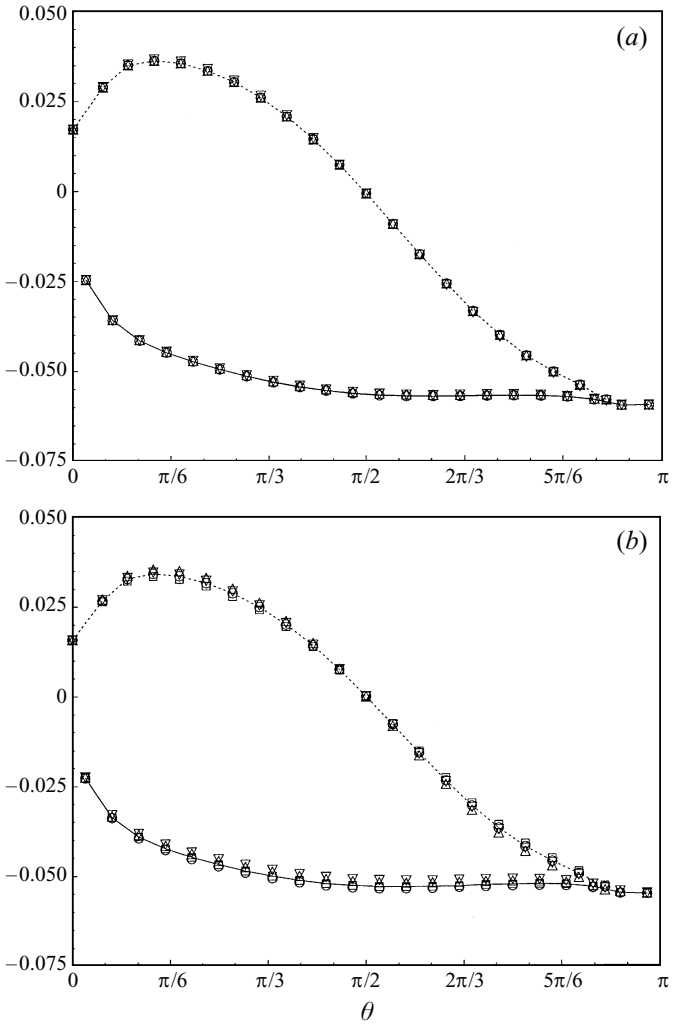

FIGURE 15. Distribution of the tangential velocities $v_\theta^*(\theta,\phi)$ and $\tilde{v}_\phi(\theta,\phi)/\sin\phi$ for $Re = 0.1$ and (*a*) $Sr = 0.02$, (*b*) $Sr = 0.2$. -----, $v_\theta^*(\theta,\phi=0)$; ——, $\tilde{v}_\phi(\theta,\phi=\frac{1}{2}\pi)$. ○, $\phi=\frac{1}{6}\pi$; □, $\phi=\frac{1}{3}\pi$; △, ϕ, $\frac{2}{3}\pi$; ▽, $\phi=\frac{5}{6}\pi$.

comparing numerical and analytical values of $\tilde{v}_\theta$ just outside the boundary layer but Auton only calculated the tangential velocities right on the sphere). Compared to Auton's theory, this positive difference in $\tilde{v}_\theta$ balances approximately the negative difference observed in $V_{U\theta}(\theta)$, leading to values of the product $\tilde{v}_\theta V_{U\theta}$ which are very close. The remark is important in view of the next section because it is easy to show (see Auton 1987) that at first order in Sr the lift force results from the integration of the product $\rho\tilde{v}_\theta V_{U\theta}$ on the bubble. It is also observed in figure 13 that when the Reynolds number increases, $\tilde{v}_\theta$ becomes more and more negative close to $\theta = 0$ and more and more positive close to $\theta = \pi$. This means that in the symmetry plane $z = 0$ the front stagnation point moves upwards (i.e. towards increasing y) when Re increases while the rear stagnation point moves downwards. This behaviour can be also clearly observed in figure 4(*c*). When the Reynolds number decreases the distributions of both $\tilde{v}_\theta(\theta,0)$ and $\tilde{v}_\phi(\theta,\frac{1}{2}\pi)$ tend to become symmetric with respect to the equatorial plane

$\theta = \frac{1}{2}\pi$. In contrast to the magnitude of $\tilde{v}_\theta(\theta, 0)$ which is roughly maintained, the magnitude of $\tilde{v}_\phi(\theta, \frac{1}{2}\pi)$ decreases by several orders, as could be anticipated from figure 9. Figures 13 and 14 show that at low Reynolds number (see especially $Re = 0.1$), both tangential components approach the creeping flow solution (13*a*). However, it is known that under such conditions the lift force results from small but non-zero inertia effects. In order to estimate properly these effects it is useful to use (13*a*) and to write the meridian velocity $\tilde{v}_\theta$ in the form

$$\tilde{v}_\theta(\theta, \phi) = (\sin^2\theta + v_\theta^*(\theta, \phi))\cos\phi. \tag{13b}$$

The tangential components $v_\theta^*(\theta, \phi)$ and $\tilde{v}_\phi(\theta, \phi)/\sin\phi$ corresponding to $Re = 0.1$ are plotted in figures 15(*a*) and 15(*b*) for $Sr = 0.02$ and $Sr = 0.2$, respectively. Both components now have a comparable order of magnitude. A comparison of the two figures reveals that for the cases considered here both the amplitude and the θ-dependence of $v_\theta^*(\theta, \phi)$ and $\tilde{v}_\phi(\theta, \phi)/\sin\phi$ are only very slightly dependent on Sr. Moreover, the azimuthal variation of both quantities is small even for $Sr = 0.2$. This result contrasts with the one displayed by figure 12(*b*) for $Re = 1$. Summarizing the behaviour revealed by figures 11(*b*), 12(*b*) and 15(*b*) one can thus conclude that the azimuthal dependence of $\tilde{v}_\phi$ is generally proportional to $\sin\phi$ except around $Re = 1$ where viscous effects and inertia effects are of similar importance.

5. The hydrodynamic forces

5.1. *Pressure and viscous stress distributions*

As is customary, the distribution of pressure and viscous effects at the bubble surface can be studied by defining a pressure coefficient C_p and a viscous stress coefficient C_n through

$$C_0(\theta, \phi) = \frac{P(\theta, \phi) - P_\infty}{\frac{1}{2}\rho U_0^2}, \quad C_n(\theta, \phi) = \frac{(\boldsymbol{n}\cdot\boldsymbol{\tau}\cdot\boldsymbol{n})(\theta, \phi)}{\frac{1}{2}U_0^2}. \tag{14}$$

In (14) P_∞ is a reference pressure chosen on the upstream boundary. Both coefficients are plotted in figure 16 for various values of the Reynolds number. In contrast with the more familiar distribution of the viscous stress on a solid sphere, C_n reaches its maximum at $\theta = 0$ and $\theta = \pi$ because the local strain rate of the flow is maximum in the stagnation regions. For the two shear rates $Sr = 0.02$ and $Sr = 0.2$ it appears that C_p and C_n depend only weakly on ϕ. In other words the distribution of both coefficients is close to the one corresponding to a uniform flow ($Sr = 0$). At moderate to high Reynolds number the azimuthal dependence of C_p is maximum near the equator of the bubble ($\theta = \frac{1}{2}\pi$), while this maximum is located near $\theta = \frac{1}{2}\pi$ and $\theta = \frac{3}{4}\pi$ at low Reynolds number. Concerning C_n, the maximum azimuthal dependence occurs near $\theta = \frac{1}{4}\pi$ and $\theta = \frac{3}{4}\pi$ whatever the Reynolds number. As could be expected, the variation of C_p and C_n with respect to ϕ becomes more important when the shear rate increases but it remains much weaker than the variation with respect to θ, even for $Sr = 0.2$. This fact suggests that if the bubble were allowed to deform, its deformation would remain much weaker along the ϕ-direction than along the θ-direction, i.e. the bubble would not depart strongly from an axisymmetric shape. Nevertheless one cannot conclude that in that case the lift force experienced by the bubble would remain unaltered: as pointed out in §2 the bubble would then rotate and the computations performed by Ervin & Tryggvason (1994) and Takagi & Matsumoto (1995) for a deformable bubble rising in a shear flow show that the sign of the lift force can reverse when the Weber number exceeds a certain value.

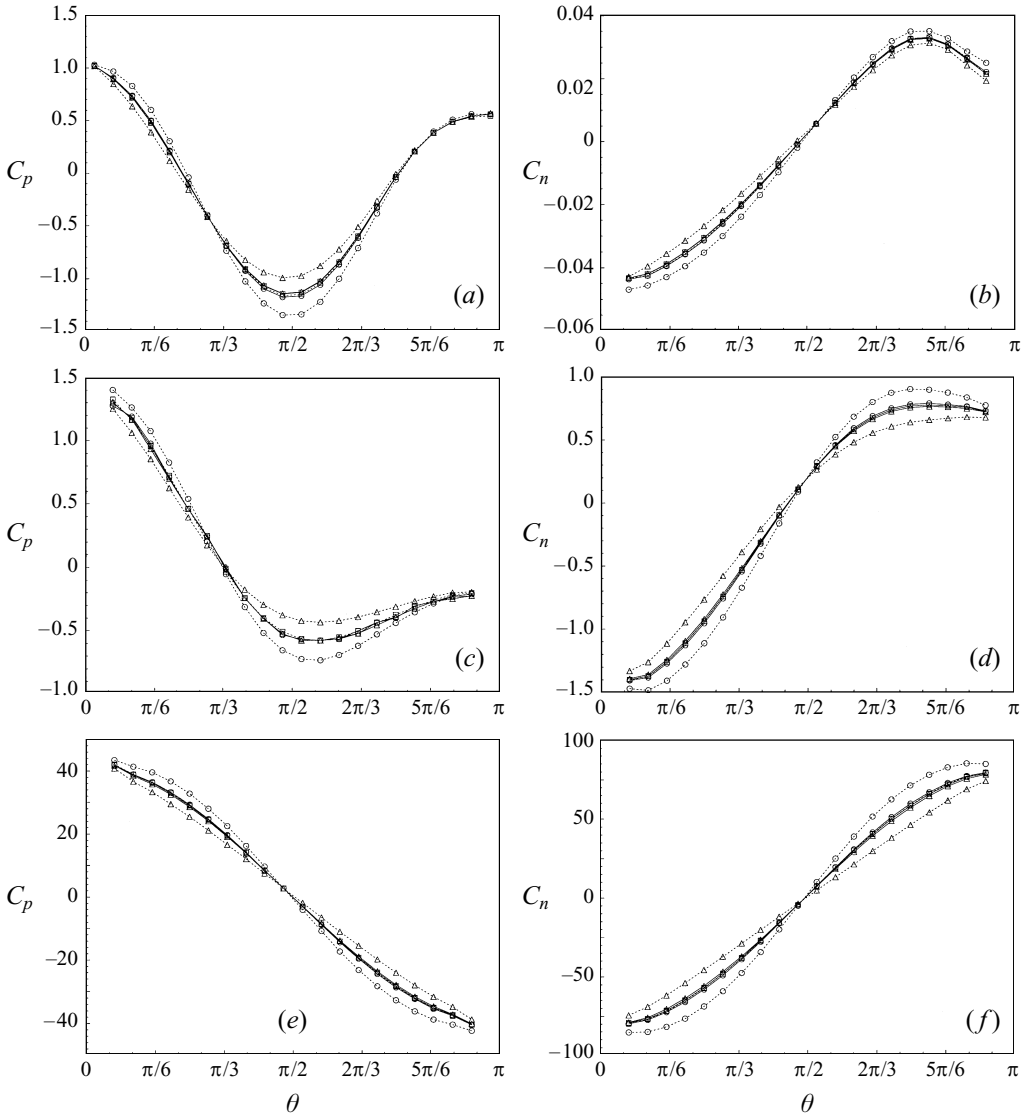

FIGURE 16. Distribution of the surface coefficients for $Sr = 0.02$ and $Sr = 0.2$. (*a*) C_p for $Re = 500$; (*b*) C_n for $Re = 500$; (*c*) C_p for $Re = 10$; (*d*) C_n for $Re = 10$; (*e*) C_p for $Re = 0.1$; (*f*) C_n for $Re = 0.1$. ——, $Sr = 0.02$; ·····, $Sr = 0.2$. ○, $\phi = 0$; □, $\phi = \frac{1}{2}\pi$; △, $\phi = \pi$.

5.2. *The drag force*

The numerical values of the drag coefficient $C_D(Re, Sr)$ are reported in table 4 for Reynolds numbers ranging between 0.1 and 500 and for the two shear rates $Sr = 0.02$ and $Sr = 0.2$. These values are compared with the drag coefficient $C_{DU}(Re)$ computed at the same Reynolds number and on the same (ζ, ψ)-mesh for a uniform flow corresponding to $Sr = 0$. It may first be noted that C_{DU} is in excellent agreement with the theoretical expressions for the drag force: for $Re \geqslant 100$ the difference between the computations and Moore's (1963) theory is less than 1% while for $Re = 0.1$ the difference with the low-Reynolds-number theory of Taylor & Acrivos (1964) is less than 0.2%. The comparison between C_D and C_{DU} reveals that for such shear rates the

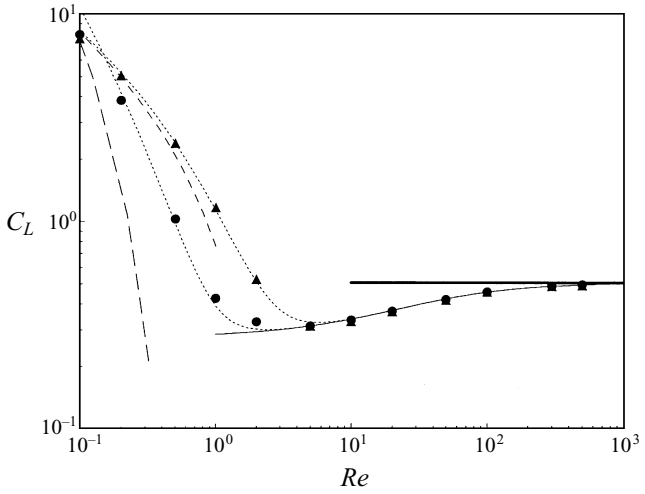

FIGURE 17. Lift coefficient C_L *vs.* *Re*. ●, $Sr = 0.02$; ▲, $Sr = 0.2$; ——, equation (8*b*) for $Sr = 0.02$; -----, (8*b*) for $Sr = 0.2$; ——, $C_L = 0.5$, (7*b*); ——, (15); ·····, (18).

		$Sr = 0.02$		$Sr = 0.2$	
Re	C_{DU}	C_D	$\lvert 1 - C_{DU}/C_D \rvert$	C_D	$\lvert 1 - C_{DU}/C_D \rvert$
0.1	162.2	162.1	0.001	162.2	0.001
0.2	82.3	82.4	0.001	82.4	0.001
0.5	33.6	33.5	0.003	33.7	0.003
1	17.4	17.5	0.006	17.5	0.006
2	9.31	9.30	0.001	9.32	0.001
5	4.27	4.25	0.005	4.29	0.005
10	2.43	2.42	0.004	2.44	0.004
20	1.403	1.396	0.002	1.403	0
50	0.670	0.669	0.002	0.673	0.004
100	0.373	0.374	0.004	0.377	0.011
300	0.141	0.142	0.007	0.145	0.021
500	0.0880	0.0889	0.010	0.0918	0.055

TABLE 4. Drag coefficients C_D in the range $0.1 \leqslant Re \leqslant 500$ for $Sr = 0.02$ and $Sr = 0.2$

effect of the shear on the drag force is very small: the relative difference between both coefficients is found to be less than 1% for $Sr = 0.02$ and less than 5% for $Sr = 0.2$. The same conclusion was reached by Dandy & Dwyer (1990) for a solid sphere subjected to similar shear rates at Reynolds numbers ranging between 0.1 and 100. The explanation of this behaviour is given by the surface distributions plotted in figure 16: since the azimuthal variations of C_p and C_n are nearly symmetric with respect to the midplane $\phi = \frac{1}{2}\pi$ and since their meridian distribution in this plane is very close to the one found in uniform flow, the change experienced by the drag force is very small. The values reported in table 4 show that the existence of the shear leads generally to a small increase of the drag force. At low Reynolds number this conclusion agrees qualitatively with the result of Harper & Chang (1968) who generalized the work of Saffman (1965) by calculating the drag and the lift induced by the shear on a solid sphere moving in an arbitrary direction. In all cases they found an increase of C_D proportional to $(Sr/Re)^{1/2}$. Unfortunately no quantitative comparison can be made with their

(*a*)

	$Sr = 0.02$			$Sr = 0.2$		
Re	C_{LP}	$C_{L\nu}$	C_L	C_{LP}	$C_{L\nu}$	C_L
0.1	2.83	4.05	7.97	2.92	4.71	7.63
0.2	1.61	2.23	3.84	2.01	3.05	5.06
0.5	0.669	0.352	1.02	1.12	1.25	2.37
1	0.461	−0.040	0.421	0.709	0.458	1.16
2	0.419	−0.093	0.325	0.489	0.0310	0.520
5	0.402	−0.0931	0.309	0.402	−0.0928	0.309
10	0.403	−0.0730	0.330	0.401	−0.077	0.324
20	0.413	−0.0493	0.364	0.413	−0.0513	0.362
50	0.442	−0.0279	0.414	0.443	−0.0300	0.412
100	0.469	−0.0178	0.451	0.467	−0.0176	0.450
300	0.490	−0.0077	0.482	0.487	−0.0076	0.480
500	0.493	−0.0049	0.488	0.489	−0.0050	0.484

(*b*)

Re	0.1	0.2	0.5	1	2
C_{LP}	2.20	1.59	1.08	0.805	0.581
$C_{L\nu}$	3.43	2.20	1.16	0.629	0.181
C_L	5.63	3.79	2.24	1.43	0.762

TABLE 5. Lift coefficient C_L, pressure contribution C_{LP}, and viscous contribution $C_{L\nu}$: (*a*) in the range $0.1 \leqslant Re \leqslant 500$ for $Sr = 0.02$ and $Sr = 0.2$; (*b*) in the range $0.1 \leqslant Re \leqslant 2$ for $Sr = 0.5$

theoretical result because, as will be shown in §5.4, Saffman's hypotheses are not appropriate in the present case. Nevertheless, the important practical conclusion is that, compared to the Stokes drag which is proportional to Re^{-1}, this drag increase is generally negligible. To summarize, there is undoubtedly an effect of the shear on the drag force but this effect is very weak for low to moderate values of the shear rate. This allows us to conclude that the drag laws established in uniform flow can be used without modification for most practical predictions of bubble motions in shear flows. We will come back on that point in §7 when discussing the case of higher shear rates at high Reynolds number.

5.3. *The lift force at moderate to high Reynolds number*

Figure 17 displays the values of the steady lift coefficient C_L in the range $0.1 < Re < 500$ for the two shear rates $Sr = 0.02$ and $Sr = 0.2$. The corresponding values of C_L and the respective contributions of pressure (C_{LP}) and normal viscous stress ($C_{L\nu}$) to the lift coefficient are reported in table 5(*a*). It is first interesting to notice that while $C_{L\nu}$ is positive at low Reynolds number, it becomes negative when the Reynolds number is larger than unity, meaning that viscous effects tend then to lower the net lift force. No simple explanation of this change of sign emerges because $C_{L\nu}$ is entirely due to the secondary velocity field produced by the asymmetry of the unperturbed flow. It is interesting to notice that for a solid sphere (for which $C_{L\nu}$ results from shear stresses), the sign of $C_{L\nu}$ is controversial. In their computations, Dandy & Dwyer (1990) found that $C_{L\nu}$ was always positive and represented the major contribution to C_L whatever the Reynolds number. In contrast, Kurose & Komori (1997) found that $C_{L\nu}$ became negative beyond a critical value of the Reynolds number slightly larger than 5.

For Reynolds numbers larger than 5 the lift coefficient C_L is found to increase continuously with Re and to tend quickly towards Auton's (1984, 1987) solution $C_{L\infty} = 0.5$ which is *a priori* valid for an inviscid fluid in the limit $Sr \to 0$. The difference between the numerical values and the inviscid solution is about 10 % at $Re = 100$, 3 %

at $Re = 300$ and 2% at $Re = 500$. Moreover, the values reported in table 5(a) show that the lift force is completely dominated by inertial effects as soon as $Re > 50$: while C_{L_ν} contributes roughly 30% of C_L when $Re = 5$, it contributes only 6% when $Re = 50$ and less than 1% when $Re = 500$. For that value of Re one finds $C_{LP} = 0.493$ for $Sr = 0.02$ so that the difference between the numerical value of the pressure contribution and the inviscid result is 1.4%. Moreover, it must be kept in mind that C_{LP} also contains a small viscous contribution resulting from the existence of the boundary layer associated with the shear-free condition (3b). There is no rigorous way to split C_{LP} into an inertial contribution and a viscous one. However, at low Reynolds number it can be shown that $C_{L_\nu} = 2C_{LP}$ (see equations (10) and (11) of Legendre & Magnaudet 1997). Moreover, a similar result holds in uniform flow for the drag force at both low and high Reynolds number ($C_{D_\nu} = 2C_{DP}$) and this result is also approximately valid at intermediate Reynolds numbers (see Magnaudet *et al.* 1995). On these grounds it seems reasonable to assume that the viscous contribution in C_{LP} is nearly equal to $C_{L_\nu}/2$ whatever the Reynolds number. If one accepts this assumption, one finds that at $Re = 500$ the inertial part of C_L is equal to 0.496 for $Sr = 0.02$ and to 0.492 for $Sr = 0.2$. These results are in almost perfect agreement with Auton's theory in the limit $Sr \to 0$. If the foregoing assumption is used to estimate the inertial part of C_{LP} for $Re > 5$, one finds that this contribution is nearly equal to 0.45 for $5 \leqslant Re \leqslant 50$ and that it increases continuously from 0.45 to 0.50 for $50 < Re \leqslant 500$. These estimates suggest that the inertial part of C_L evolves very slowly with the Reynolds number for $Re \geqslant 5$. Present results demonstrate that the inviscid theory applies in the present range of shear rates as soon as the Reynolds number exceeds several hundred, despite the fact that the surface distributions of $V_{U\theta}(\theta)$ and $\tilde{v}_\theta(\theta, \phi)$ examined in §4 show that viscous effects affect significantly the local quantities even for $Re = 500$.

One of the most prominent features revealed by figure 17 is that in the range of Sr considered here, C_L is virtually independent of Sr for $Re > 5$. In contrast, a strong influence of the shear rate is observed for $Re < 5$. This result indicates that for $Re > 5$ and $Sr \leqslant 0.2$ (at least), the magnitude of the lift force is directly proportional to the vorticity of the undisturbed flow. The numerical results corresponding to this range of parameters can be fitted by the empirical correlation

$$C_L^{\text{high Re}}(Re) = \frac{1}{2}\frac{1 + 16Re^{-1}}{1 + 29Re^{-1}}. \tag{15}$$

The curve corresponding to relation (15) is shown on figure 17. It fits the numerical results with an accuracy better than 1%. At high Reynolds number (15) tends towards $0.5\ Re^{-1}$–$6.5\ Re^{-1}$, showing that the difference between C_L and $C_{L\infty}$ decreases as Re^{-1}. This difference obviously comes from viscous effects and the negative sign of the corresponding coefficient reflects the fact that C_{L_ν} is negative. It is not very surprising to find that the viscous contribution to the lift force behaves like Re^{-1} for large values of Re since this evolution corresponds to the well-known behaviour of the drag force, i.e. $C_{DU_{Re\to\infty}} = 48\ Re^{-1}$ (Levich 1962, p. 445).

5.4 *The lift force at low to moderate Reynolds number*

Figure 18 shows in detail the evolution of the lift coefficient for moderate to low Reynolds numbers ($0.01 < Re < 10$). When the Reynolds number decreases, C_L reaches a minimum roughly equal to 0.3 around $Re = 5$. Then for lower Reynolds numbers the lift coefficient increases continuously and very strongly when Re

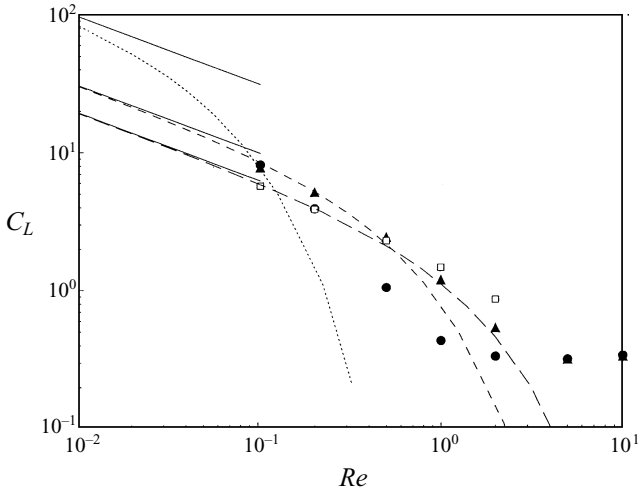

FIGURE 18. Lift coefficient C_L *vs.* Re in the range $0.01 < Re < 1$. ●, $Sr = 0.02$; ▲, $Sr = 0.2$; □, $Sr = 0.5$. ·····, (8*b*) for $Sr = 0.02$; -----, (8*b*) for $Sr = 0.2$; ——, (8*b*) for $Sr = 0.5$; ——, (8*b*) using the value $J(\infty)$ corresponding to Saffman's assumption.

decreases. Moreover, in contrast to the behaviour observed for $Re > 5$, figures 17 and 18 reveal that C_L is greatly dependent on the shear rate in this range of Reynolds number. This dependence is quite complex as suggested by the analytical solution (8*b*): the lift coefficient corresponding to $Sr = 0.02$ is larger than the one corresponding to $Sr = 0.2$ for $0.2 \leqslant Re \leqslant 5$ but it becomes smaller at lower values of Re. Not surprisingly the viscous contribution $C_{L\nu}$ becomes important and even dominant when the Reynolds number is smaller than unity. As shown by the Low-Reynolds-number analytical solution, both C_{LP} and $C_{L\nu}$ make positive contributions to the lift force at such Reynolds numbers.

A good agreement between the numerical values of C_L and the analytical solution (8*b*) is observed for $Sr = 0.2$ when $Re < 0.5$. In contrast no agreement is obtained for $Sr = 0.02$ over the whole range of Re covered by the present computations, except perhaps at $Re = 0.1$ (but that result must be taken with caution, see §3). These results deserve some comments concerning the validity of the solution (8*b*). The asymptotic study of the low-Reynolds-number equations shows that in the present flow the creeping flow solution becomes invalid at a distance $R_S = O(2R(Sr\,Re)^{-1/2})$ (Saffman's radius) owing to the small inertia effects induced by the shear, and at a distance $R_O = O(2R\,Re^{-1})$ (Oseen's radius) owing to the usual inertia effects resulting from the mean flow. Saffman (1965) developed his solution under the assumption $R_O \quad R_S$. McLaughlin (1991) extended his work by assuming that R_O is larger than R_S or at least of the same order as R_S. In both cases the shear is responsible for the first invalidity of the creeping flow solution. However, when the shear is small enough or the Reynolds number is large enough, this first invalidity is caused by the mean flow. In other words it is Oseen's solution, not Stokes' solution, which is modified by the shear in that case. The ratio $\varepsilon = R_O/R_S = (Sr/Re)^{1/2}$ is thus a crucial parameter for all these asymptotic solutions and especially for the solution (8*b*) based on McLaughlin's assumption. For example for $Sr = 0.02$ the function $J(\varepsilon)$ which appears in (8*b*) becomes negative when $Re > 0.4$ ($\varepsilon \approx 0.22$), implying a negative lift force. This prediction is obviously unphysical. It only stresses the fact that the asymptotic solution is invalid for such values of the physical parameters. For $Sr = 0.02$ and $Re = 0.1$ one gets $\varepsilon \approx 0.45$, a

value which is probably already out of the range of validity of (8*b*). In contrast, for similar Reynolds numbers ε reaches significantly higher values when $Sr = 0.2$: one gets $\varepsilon = 0.71$ for $Re = 0.4$ while $Re = 0.1$ corresponds to $\varepsilon = 1.41$. A comparison of the numerical results with the predictions of (8*b*) suggests that the lower bound of validity of the asymptotic solution is $\varepsilon \approx 0.7$. Obviously this comparison also shows that Saffman's hypothesis (which leads to the use of the value of J corresponding to $\varepsilon \to \infty$ in (8*b*)) is never satisfied in the present context. The predictions given by Saffman's assumption correspond to the straight lines plotted in the range $0.01 \leqslant Re \leqslant 0.1$ in figure 18. By extrapolating these lines one sees clearly that none of the numerical results plotted in figure 18 agrees with that theory because the values of ε used in the computations are always moderate. For example for $Sr = 0.2$ one finds that McLaughlin's assumption gives a valid prediction for $Re \leqslant 0.4$ while Saffman's and McLaughlin's results begin to agree only for $Re \leqslant 0.03$. These results lead us to conclude that the theoretical prediction (8*b*) is valid for $\varepsilon \geqslant 0.7$ and at least up to $Re = 0.4$. However, the choice $Sr = 0.2$ is somewhat limiting because in the range $0.4 \leqslant Re \leqslant 1$ the values of ε fall below 0.7. To avoid this limitation, additional computations were performed in the large $0.1 \leqslant Re \leqslant 2$ with a larger value of Sr, namely $Sr = 0.5$ which leads to $\varepsilon \approx 0.7$ for $Re = 1$. The corresponding results are also reported in figure 18 and in table 5(*b*). It can be seen in figure 18 that the values of C_L found for $Re < 0.5$ agree very well with the asymptotic result (8*b*) (the error being within 1%) while the values found for larger values of Re are clearly larger than the asymptotic prediction. This finding suggests that $Re \approx 0.5$ is the intrinsic limit of validity of (8*b*), even for large shears. Therefore, combining the above indications allows us to conclude that the asymptotic solution (8*b*) is valid for $Re \leqslant 0.5$ and $\varepsilon \geqslant 0.7$, i.e. $Sr \geqslant 0.5\, Re$.

Having discussed the limitations of the analytical solutions we must stress again the difficulties related to the confinement effect observed in the computations. It was clearly established in §3 that for $Re = 0.1$ the size of the computational domain influences the numerical results corresponding to $Sr = 0.02$. This is also apparent in figure 18 because if the numerical 'curve' is extrapolated towards lower values of Re, the extrapolated values lie well below the theoretical curve, even when (8*b*) becomes valid, i.e. for $Re \leqslant 0.05$. Concerning the results corresponding to $Sr = 0.2$, one may also suspect that small confinement effects appear when $Re = 0.1$ because the numerical result lies slightly below the theoretical curve for this Reynolds number. In contrast no confinement effect is discernible for $Sr = 0.5$, even when $Re = 0.1$, because in that case one has $R_S/R \approx 9$ so that the lift force can be correctly evaluated with the present grid. Keeping in mind that the computational domain extends up to 100 bubble radii when $Re = 0.2$ and 0.1, it appears that the accurate computation of the lift force at low Reynolds number has a very high computational cost because it requires very large domains. Thus there is almost no doubt that the low-Reynolds-number results found by Dandy & Dwyer (1990) for a solid sphere using a small domain extending only up to 25 sphere radii were contaminated by this confinement effect and that their agreement with Saffman's prediction was fortuitous. If one wants to avoid very large computational times, the range of parameters over which the numerical predictions can be compared properly with the theory is quite narrow because the former are easily obtained for 'not too large' values of Sr and 'not too small' values of Re while the latter is valid only for small enough values of Re and large enough values of Sr/Re. Despite this limitation the agreement observed in the present study for $Sr = 0.2$ and above all for $Sr = 0.5$ is sufficient for concluding that (8*b*) is indeed the correct asymptotic expression of the lift force for small enough Re.

Coming back to the numerical results, it might be interesting to fit them by a correlation extending the range of validity of (8*b*). For that purpose the function $J(\varepsilon)$ tabulated numerically by McLaughlin (1991) must be replaced by some empirical function $J'(\varepsilon)$ so that one can write

$$C_L^{\text{low Re}}(Re, Sr) = \frac{6}{\pi^2}(Re\,Sr)^{-1/2}J'(\varepsilon). \tag{16}$$

The function $J'(\varepsilon)$ is determined in such a way that it agrees with the present results corresponding to $Sr = 0.2$ and 0.5 for $Re < 1$ and that it tends towards $J(\varepsilon)$ for $\varepsilon > 0.8$ (for which the difference between (8*b*) and the computational results is less than 1 %). One gets

$$J'(\varepsilon) = \frac{J(\infty)}{(1+0.2\varepsilon^{-2})^{3/2}}, \tag{17}$$

where $J(\infty) = 2.255$. One can notice that $J'(\varepsilon)$ is always positive and that it tends to zero when $Re \to \infty$. It is now possible to combine the expressions (15) and (16)–(17) in order to obtain a purely empirical correlation valid whatever the Reynolds number. A very simple and accurate expression is found to be

$$C_L(Re, Sr) = ([C_L^{\text{low Re}}(Re, Sr)]^2 + [C_L^{\text{high Re}}(Re)]^2)^{1/2}. \tag{18}$$

This correlation matches the analytical solutions in both limits $Re \to 0$ and $Re \to \infty$. One sees in figure 17 that the curves corresponding to (18) are in very good agreement with the numerical results over the whole range of Re.

Finally it is worth noting that most of the results discussed in this subsection also apply for a solid sphere since it was shown by Legendre & Magnaudet (1997) that at low Reynolds number the physical difference between a bubble and a solid sphere modifies the lift force only by a numerical factor 4/9. In particular the bounds of validity of (8*b*) established above and the correlation (16)–(17) are certainly approximately valid for a solid sphere provided the numerical factor 6 in (8*b*) and (16) is replaced by 27/2.

5.5. *The origin of the lift force and its evolution with the Reynolds number*

The numerical results discussed in the foregoing subsections give a quite complete view of the various contributions to the lift force and they show in detail its evolution with the Reynolds number. However they mask somewhat the origins of the lift force and more precisely the differences existing between the mechanisms responsible for its low- and high-Re behaviour. This origin is more apparent in the theoretical expressions (7)–(8) and we should devote some lines to the similarities and the differences existing between the two types of asymptotic behaviour. The expression established by Auton (1984, 1987) (or more precisely the integral giving the lift force, see equation (5.3) of Auton (1987)) shows that for the simple shear flow considered here, a lift force appears in inviscid fluid because the advection and the stretching of the basic vorticity $-\alpha \boldsymbol{e}_z$ contained in the unperturbed flow are non-symmetric around the bubble (with respect to the plane $y = 0$), resulting in a non-symmetric distribution of the meridian velocity at the bubble surface. In contrast, expression (8*a*) makes clear the fact that at low Reynolds number the lift force is proportional to the drag F^0. As shown by Saffman (1965) the far-field flow sees the bubble (and more generally the body) as a point source of momentum whose strength is F^0. This momentum source induces velocities which are non-symmetric with respect to $y = 0$ because they are advected non-symmetrically by the unperturbed flow. These velocities and the associated pressure field then result

in a correction to the primary force F^0 which is not aligned with the direction of the primary flow. Up to that point, vorticity has not been invoked in that mechanism. However, it is well known that in low-Reynolds-number flows the drag force is directly proportional to the strength of the vorticity present at the surface of the body. Then it becomes clear that the low-Reynolds-number lift force results from the existence of a non-zero vorticity at the surface of the body and from the asymmetric advection produced by the shear. If one compares the two mechanisms it appears now that they have in common two essential ingredients, namely vorticity and asymmetric advection with respect to the plane $y = 0$. The central difference between them is the origin of the vorticity. In the former (which may be called the Lighthill–Auton mechanism) vorticity comes necessarily from the unperturbed flow because it cannot be generated at the surface of the body. In contrast in Saffman's mechanism the outer vorticity associated with the shear plays no role: the shear is essential in the mechanism because it makes the advective process non-symmetric but the vorticity is provided by the shear-free (or the no-slip) condition at the surface of the body. According to the shape of the function $C_L(Re)$ displayed by figure 17, Saffman's mechanism clearly dominates for Reynolds numbers less than unity. Then in an intermediate range of Re, say $1 \leqslant Re \leqslant 20$, the vorticity generated at the bubble surface and that present in the outer flow are both active. For larger values of Re the inviscid mechanism is clearly dominant and the vorticity generated at the bubble surface no longer plays a significant role. This discussion also makes clear the key difference between the evolution of the lift force on a clean bubble and on a solid sphere. For a solid sphere the low-Reynolds-number behaviour is identical to that corresponding to a bubble. In contrast, when Re increases, the magnitude of the vorticity generated by the no-slip condition increases like $Re^{1/2}$ while the vorticity generated by the shear-free condition on a spherical bubble never exceeds $3U_o/R$ in a uniform flow. Thus in the case of a solid sphere, the surface vorticity becomes so intense when Re goes beyond some value that it probably overwhelms the outer vorticity in the mechanism generating the lift force and the two kinds of bodies behave completely differently.

Having discussed the evolution of C_L with Re, it is interesting to study the evolution of the ratio between the lift force and the drag force because this ratio gives an idea of the relative influence of the various forces acting on the bubble. According to the definition (6), the ratio F_L/F_D can be simply expressed as

$$\frac{F_L}{F_D} = \frac{4}{3} Sr \frac{C_L}{C_D}. \tag{19}$$

The quantity $Sr^{-1}F_L/F_D$ is plotted as a function of Re in figure 19. As could be expected this plot reveals two different types of behaviour. At small to moderate Reynolds number the lift force is very small compared to the drag force and the ratio F_L/F_D is roughly constant for a given shear rate. In contrast, for $Re \geqslant 5$ this ratio increases continuously with Re and the lift force becomes comparable to and even larger than the drag force at high Reynolds number. For example for $Sr = 0.2$, one finds $F_L \approx 0.013F_D$ at $Re = 0.1$ and $F_L \approx 1.4F_D$ at $Re = 500$. This evolution underlines the fact that the lift force and more generally the forces related to inertia are tremendously important for predicting the motion of bubbles. For $Re \geqslant 5$ figure 19 shows that F_L/F_D grows linearly with Re. This behaviour comes simply from the fact that, in that range of Re, C_L is nearly constant while C_D decreases as Re^{-1}.

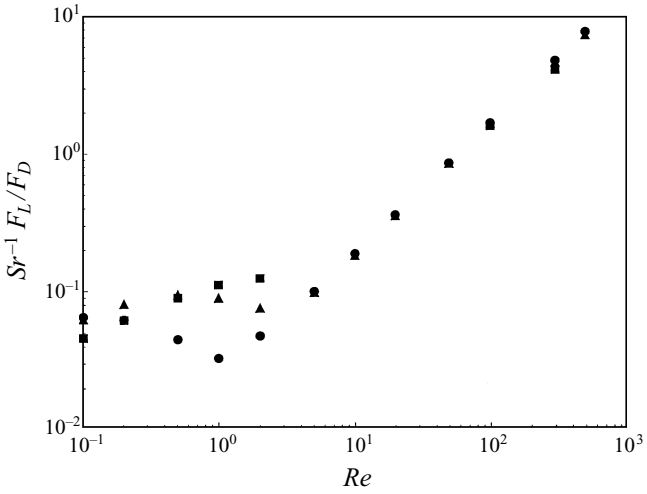

FIGURE 19. Ratio of the lift and drag forces $Sr^{-1}F_L/F_D$ *vs. Re.* ●, $Sr = 0.02$; ▲, $Sr = 0.2$; ■, $Sr = 0.5$.

6. The transient behaviour of the lift force

Up to now we have only considered the steady results of the computations. However, it is also of interest to examine the evolution of the lift force during the transient stages following the beginning of the computations. Let us recall that the initial velocity field used throughout this work corresponds to the undisturbed velocity $\boldsymbol{U}$ defined by (1). In other words the bubble is suddenly introduced in the flow at time $t = 0$. Since the numerical algorithm satisfies incompressibility at each time step, the computed flow is physically meaningful whenever $t > 0$. Just after the introduction of the bubble the velocity field is composed of the undisturbed flow $\boldsymbol{U}$ plus an irrotational correction $\boldsymbol{V}_p$ ensuring the impermeability condition at the bubble surface, i.e. $(\boldsymbol{U}+\boldsymbol{V}_p)\cdot\boldsymbol{n} = 0$. The reason why the lift force (and also of course the drag force) does not immediately reach its steady value is obviously related to the finite time required by the vorticity to be advected, stretched and diffused around the bubble. To study the effect of these processes on the lift force it is convenient to define two different time scales, according to the value of the Reynolds number. The advective time scale $t_a = R/U_o$ is obviously relevant at high Reynolds number. At low Reynolds number the distance which must be considered is not the bubble radius but Saffman's radius $R_S = 2R(Sr\,Re)^{-1/2}$ at which Stokes' solution is modified by inertia effects. Consequently for such Reynolds numbers the relevant time scale seems to be $t_\nu = R_S^2/\nu$ which is the time required by the vorticity perturbation produced by the bubble to reach the distance R_S. Intuitively one expects the lift force to reach its steady value in a time which scales with t_ν (resp. t_a) at low (resp. high) Reynolds number. In the low-Re limit it does not seem surprising that a relaxation effect may affect the lift force because one is familiar with a similar process affecting the drag force, the so-called Basset–Boussinesq force for a solid sphere. In contrast, in the inviscid limit the situation deserves some comments. If in place of a sphere one considers a two-dimensional body (say a cylinder) in the flow field (1), one finds that the lift force on this body immediately reaches its steady value. This is due to the fact that the initial vorticity field is constant and that no vortex stretching can occur in that case since the flow is strictly two-dimensional. Then it is straightforward to show that the introduction of the cylinder leaves the initial vorticity field unchanged so that the velocity field $\boldsymbol{U}+\boldsymbol{V}_p$ defined above is the steady solution

of the problem (see Auton, Hunt & Prud'homme 1988). The foregoing remark stresses the fact that in the flow field considered here, a relaxation effect can affect the lift force in the high-Reynolds-number limit only if the body is three-dimensional (this is obviously true only for a body satisfying a zero-shear-stress condition; otherwise vortex shedding would occur and this would affect the lift force even for a two-dimensional body).

To our knowledge no analytical study of the transient behaviour of the lift force on a sphere has been reported so far, either in the low-Reynolds-number limit or in the inviscid one. Most authors have considered strictly steady situations. In contrast Auton *et al.* (1988) considered a sphere moving in an unsteady rotational flow. However they assumed that the change $\Delta\omega$ experienced by the local vorticity ω during the time t_a was much smaller than ω so that the steady solution developed by Auton (1987) for the lift force produced by the shear was still applicable. The general unsteady problem is obviously very difficult to study analytically, even in the asymptotic limit $Sr \quad 1$. Nevertheless one can get useful information by calculating the value of the lift coefficient just after the introduction of the bubble, say $C_L(t = 0^+)$. This calculation is carried out in Appendix A and it is found that $C_L(t = 0^+) = 3/4$, whatever the value of the shear rate. This result holds whatever the Reynolds number because it can be easily shown that the normal viscous stresses produced by V_p lead to $C_{L\nu} = 0$ and because the initial vorticity field is uniform so that the viscous term in (2*b*) is initially zero. However, in the high-Reynolds-number limit the above result is valid for $t \quad t_a$ while at low Reynolds number, vorticity diffuses in a typical time much smaller than t_a so that the result is only valid within a much shorter time interval. From this result one can anticipate the evolution of the lift coefficient during the transient stage. At high Reynolds number C_L decreases from its initial value of 3/4 to its steady value of 1/2, meaning that advection of vorticity around the bubble lowers the lift force. At low Reynolds number, the vorticity perturbation produced by the bubble is confined at short times in the neighbourhood of the bubble. During that stage this perturbation only diffuses and one can expect this process to decrease C_L. In a second stage this perturbation begins to reach the region where inertia effects become comparable to viscous diffusion and Saffman's mechanism begins to act. Then C_L may increase or decrease in time, depending on the magnitude of the steady value given by (8*a*) (for the moderate shear rates considered here this value is quite high so that one can expect an increase of C_L).

To confirm the foregoing analysis two time evolutions of C_L are reported in figures 20(*a*) and 20(*b*). The first case corresponds to $Re = 500$ and $Sr = 0.02$ while the second one is chosen in the low-Reynolds-number regime, namely $Re = 0.5$ and $Sr = 0.5$. Figure 20(*a*) confirms the theoretical result $C_L(t = 0^+) = 3/4$ since one finds numerically $C_L(t = 0^+) \approx 0.73$. It also shows that during the transient stage C_L decreases continuously towards its steady value. This value is approximately reached at $t = 2t_a$ which corresponds to the time required by the flow to advect vorticity over one bubble diameter. In the low-Reynolds-number case, figure 20(*b*) shows clearly that C_L increases in time towards its steady value (a short period of decrease also exists at the very beginning of the motion but it is masked by the time scale of the figure). In agreement with the analysis developed above, one sees that C_L reaches its steady value after a time interval of the order of $2t_\nu$ to $3t_\nu$.

In view of the discussion below it is worth noting that we have shown that in a transient situation the value of the lift coefficient can be markedly different from the value of the added mass coefficient, i.e. $C_M = 1/2$. From a practical point of view, our results may be used to compute correctly the motion of bubbles moving in flows having

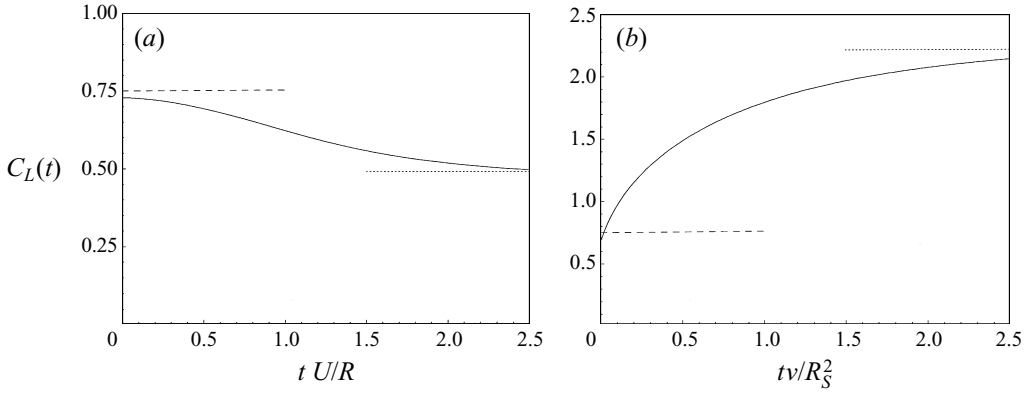

FIGURE 20. Transient behaviour of the lift coefficient at (*a*) high Reynolds number ($Re = 500$, $Sr = 0.02$), (*b*) low Reynolds number ($Re = 0.5$, $Sr = 0.5$). -----, Theoretical initial value (A 15); ·····, steady value.

sheared and unsheared regions. For example if a bubble has been moving in a region where the flow is uniform and penetrates into a sheared region, the lateral motion of the bubble is underpredicted if the steady value of the lift coefficient is used at all time. The error is negligible for large values of Re because during a time $2t_a$ the displacement of the bubble is only $2R$, i.e. one diameter. In contrast for low values of Re and Sr, the error can be much larger because during a time $2t_\nu$ the bubble moves over a distance equal to $4Sr^{-1}R$. Moreover the results discussed in this section can be of importance for determining accurately the motion of bubbles in strongly unsteady sheared flows, like oscillatory flows with shear. However, this case has to be considered specifically before any firm conclusion can be derived.

7. The effect of the shear rate on the lift and drag coefficients at high Reynolds number

It was shown in §5 that at moderate to large Reynolds number the lift coefficient is nearly independent of Sr for $Sr \leqslant 0.2$. To see whether this is also the case for larger values of the shear rate, specific computations were carried out for $Re = 300$ and $Re = 500$ at various shear rates ranging from $Sr = 0.2$ to $Sr = 1$. In order to reduce the computational cost and to avoid very large negative values of the velocity (see §3), the size of the computational domain was decreased to $R_\infty/R = 20$ in these computations (another possibility that we did not explore would have been to consider a shear flow with a uniform shear close to the bubble and a decreasing shear far from it). The resulting evolution of the lift coefficient is plotted in figure 21(*a*), the corresponding numerical values being given in table 6. The key feature displayed by figure 21(*a*) is the small but consistent decrease of C_L observed for $Sr \geqslant 0.2$. For example one finds $C_L = 0.449$ for $Re = 300$ and $Sr = 1$ while for the same Reynolds number one gets $C_L = 0.483$ for $Sr = 0.02$. The difference cannot be attributed to viscous effects because the numerical values of $C_{L\nu}$ reported in table 6 show that for a given value of Re the viscous contribution to the lift coefficient remains nearly independent of Sr; the variations of $C_{L\nu}$ are typically two orders of magnitude smaller than those of C_L. Consequently one can conclude that when Sr increases there is a decrease of C_L which is due to inertia effects, and more precisely to the nonlinearities of the vorticity equation.

The numerical results obtained for $Sr = O(1)$ could be used to correct the correlation (15) given in §5 by replacing the coefficient $1/2$ by some function of Sr. However, the

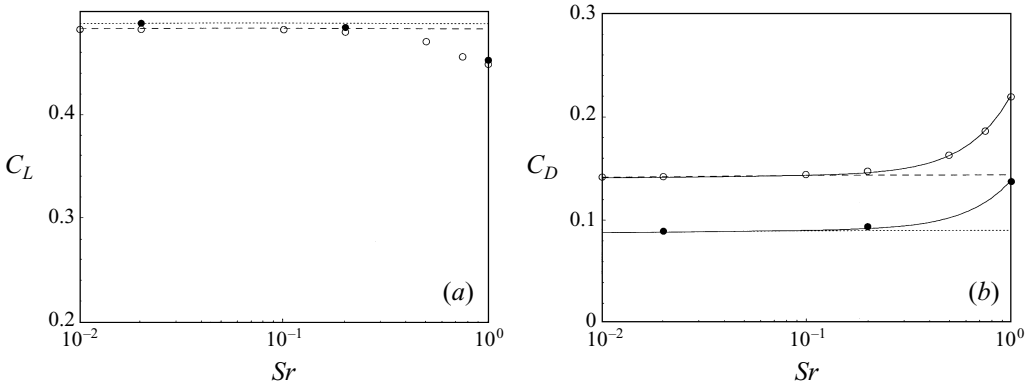

FIGURE 21. Effect of the shear rate on (*a*) the lift coefficient and (*b*) the drag coefficient at high Reynolds number. Open symbols: $Re = 300$; closed symbols: $Re = 500$; in (*b*) ——, equation (20).

Re	*Sr*	0.01	0.02	0.1	0.2	0.5	0.75	1
300	C_{LP}	0.491	0.490	0.489	0.0487	0.0478	0.465	0.456
	C_{LV}	−0.0077	−0.0077	−0.0077	−0.0076	−0.0075	−0.0077	−0.0078
	C_L	0.483	0.482	0.481	0.480	0.471	0.457	0.449
500	C_{LP}	—	0.493	—	0.489	—	—	0.457
	C_{Lv}	—	−0.0049	—	−0.0050	—	—	−0.0051
	C_L	—	0.488	—	0.484	—	—	0.452

TABLE 6. Lift coefficients C_L, pressure contributions C_{LP}, and viscous contribution C_{Lv} for $Re = 300$ and $Re = 500$ in the range $0.02 \leqslant Sr \leqslant 1$

most important practical consequence of the increase of the shear rate is found on the drag coefficient. The values of C_D obtained with the present shear rates are plotted in figure 21(*b*). One observes that the increase of C_D with Sr which is negligible for $Sr \leqslant 0.2$ becomes very significant when Sr is of order unity. For example the drag coefficient corresponding to $Re = 300$ increases by more than 54% from the value $C_D = 0.140$ for $Sr \quad 1$ until $C_D \approx 0.216$ for $Sr = 1$. Thus for such high values of the shear rate the predictions given by Moore's theory (Moore 1963) do not apply. An empirical fitting of the present results can be easily obtained by noting that since the drag force cannot depend on the sign of the shear, the difference $C_D(Re, Sr) - C_{DU}(Re)$ (C_{DU} being the value of C_D in uniform flow) is necessarily proportional to an even power of Sr. Using the data shown in figure 21(*b*) one obtains

$$C_D(Re, Sr) = C_{DU}(Re)[1 + 0.55Sr^2]. \tag{20}$$

Interestingly, the increase of the drag coefficient comes essentially from the contribution of the pressure. The values of the two contributions C_{Dv} and C_{DP} are given in table 7. It can be seen that C_{Dv} is only weakly dependent on Sr while C_{DP} increases sharply at high shear rate. This difference between the behaviour of viscous and pressure contributions is similar to that observed for the lift force. It suggests that it is essentially the modification of the pressure distribution induced by the inertia effects associated to the shear which is responsible for the drag increase. To get a better understanding of this phenomenon, the pressure distribution at the surface of the bubble is shown in figure 22 for $Sr = 1$ and $Re = 300$. Compared to the case $Sr = 0.2$, it appears that this distribution is strongly modified in the symmetry plane of the flow ($z = 0$). Roughly,

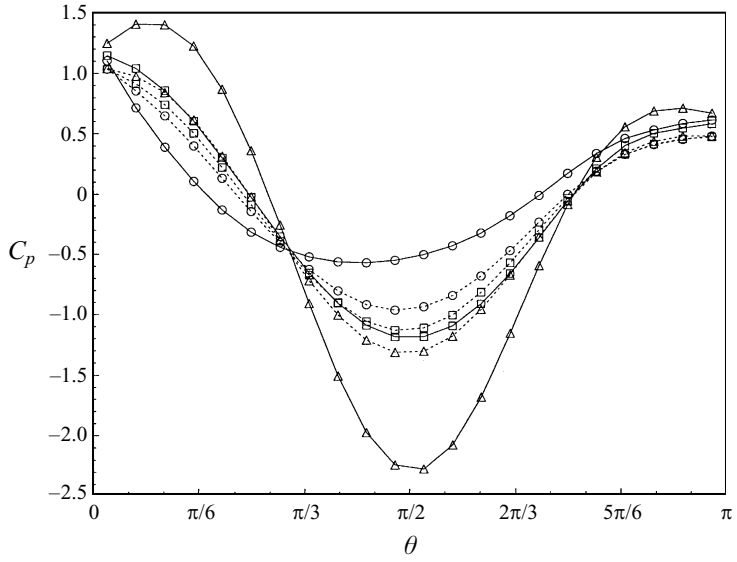

FIGURE 22. Effect of the shear rate on the distribution of C_p at the surface of the bubble ($Re = 300$). ○, $\phi = 0$; □, $\phi = \frac{1}{2}\pi$; △, $\phi = \pi$; ——, $Sr = 1$; ·····, $Sr = 0.2$.

Re	Sr	0	0.01	0.02	0.1	0.2	0.5	0.75	1
300	C_{DP}	0.0544	0.0546	0.0546	0.0553	0.0579	0.0716	0.0899	0.118
	C_{Dv}	0.0869	0.0870	0.0870	0.0871	0.0874	0.0892	0.0935	0.0976
	C_D	0.141	0.142	0.142	0.142	0.145	0.161	0.184	0.216
500	C_{DP}	0.0332	—	0.342	—	0.0368	—	—	0.0749
	C_{Dv}	0.0548	—	0.0547	—	0.0550	—	—	0.0600
	C_D	0.0880	—	0.0889	—	0.0918	—	—	0.135

TABLE 7. Drag coefficient C_D, pressure contribution C_{DP}, and viscous contribution C_{Dv} for $Re = 300$ and $Re = 500$ in the range $0.02 \leqslant Sr \leqslant 1$

three regions can be distinguished. In the front part (say $\theta < \frac{1}{3}\pi$) the pressure found for negative values of y ($\phi = \pi$) is decreased (compared to the case $Sr = 0.2$) while it is very significantly increased at the upper part of the bubble ($\phi = 0$). The maximum pressure, which corresponds to the stagnation point, is located at $\theta_o \approx \pi/12$. Overall this region provides a much larger positive contribution to the drag than in usual situations, especially because the elementary area around the position of the maximum is obviously much larger in the present case than when this maximum is located close to $\theta = 0$. In the central region (say $\frac{1}{3}\pi < \theta < \frac{3}{4}\pi$) one observes a very strong asymmetry between the distributions corresponding to the upper and lower parts of the bubble. This reflects the fact that the meridian velocity V_θ is much larger above the bubble than below it (precisely, in the present case the maximum of this velocity component is found to be 1.85 for $\phi = 0$, 1.13 for $\phi = \pi$, while it is about 1.40 in the plane $\phi = \frac{1}{2}\pi$). The contribution of this region to the drag is clearly negative and comes essentially from the lower part of the bubble where a significant asymmetry of the distribution with respect to the equatorial plane $\theta = \frac{1}{2}\pi$ is observed. Finally, at the rear of the bubble ($\theta > \frac{3}{4}\pi$), the asymmetry between the distributions found for $\phi = 0$ and $\phi = \pi$ is small, indicating that this region is much more governed by viscous effects than by the

influence of the shear. Summarizing, one concludes that, compared to the case of small shears, the front region strongly increases the drag while the central region tends to decrease it. Since the largest contribution is the increase coming from the vicinity of the stagnation point, the overall effect leads to an increase of the total pressure drag.

8. The relation between the lift coefficient and the added mass coefficient

In the introduction it was pointed out that several studies have concluded that in inviscid flow the lift coefficient C_L of a sphere is equal to its added mass coefficient C_M. It is the purpose of this section to discuss this problem in more detail and to examine the degree of generality of this equality using some results of the simulations.

In the work of Auton (1987) and Naciri (1992) (who generalized the foregoing result to ellipsoids) the lift coefficient was first obtained by solving the rotational flow around the body and the identity between C_L and C_M appeared fortuitously. To establish it on deeper grounds both authors re-derived the value of C_L by applying a momentum balance to a large cylinder of fluid surrounding the body. In that derivation the result that emerged was $C_L = C_{VM}$, C_{VM} being the drift volume coefficient defined by Darwin 1953). This result was obtained under the same assumptions as the direct calculation of C_L, namely a steady flow with Sr 1. The drift volume represents the volume limited by the initial and final positions of fluid particles lying initially in a plane normal to the displacement of the sphere and entrained by its motion. Darwin showed that when this volume is properly defined, the identity $C_M = C_{VM}$ holds for a steady irrotational unbounded flow. Later the conditions of validity of this identity were carefully examined by several authors (see especially Eames, Belcher & Hunt 1994). Summarizing, the identity $C_L = C_{VM}$ was proved by Auton (1987) and Naciri (1992) for a steady flow under the assumption Sr 1 and it implies $C_L = C_M$ if Darwin's result applies. This identity was recovered under the same physical assumptions by Wells (1993) (see also Wells 1996) who performed an elegant geometrical determination of the vorticity distribution around the sphere and evaluated the force as the rate of change of the fluid impulse.

As mentioned in the introduction, another series of works tried to make a direct link between C_L and C_M by invoking various forms of the frame indifference principle. The use of this principle has led to many conceptual or technical errors and to erroneous interpretations, some of them carefully discussed in the context of forces acting on particles by Ryskin & Rallison (1980) or by Auton (1984). These authors showed that generally, the only acceptable form of this 'principle' is the observer frame indifference (OFI) principle (Auton 1984) which states that the overall force must transform in an objective way between two different frames of reference because its magnitude cannot depend on the state of the observer. Ryskin & Rallison (1980) and Auton (1984) demonstrated that the stronger form of the frame indifference principle which states that the force can only depend on objective quantities, i.e. that its functional expression is unaffected by a solid body motion (a principle called rigid body frame indifference (RBFI) by Auton), is incorrect as soon as one considers problems in which inertia effects are strong enough to affect the microstructure of the flow. This means that the general functional form of the total hydrodynamic force acting on a sphere derived by Drew & Lahey (1979) through an extensive use of the RBFI 'principle' is not correct. In Appendix B we apply the OFI principle and we establish how the original expression found by Auton *et al.* (1988) for the hydrodynamic force on a sphere moving in an inviscid, weakly rotational flow transforms in a rotating frame of reference. We then show that no information on the lift and added mass coefficients can be found from this

expression, i.e. that the result holds whatever the values of C_L and C_M. Thus one has to conclude that no mathematical constraint like $C_L = C_M$ can be deduced from the application of the frame indifference principle.

The foregoing discussion shows that the only equality between C_L and C_M which has a sound physical meaning is the one derived by Auton (1987), Naciri (1992) and Wells (1993). Our purpose in the remainder of this section is to discuss its range of validity. Since we consider only a steady linear shear flow with a bubble at rest, no added mass force exists in the present case and C_M cannot be determined. However, it is now widely agreed that the added mass coefficient does not depend either on the strength of the acceleration or on the Reynolds number. The result $C_M = \frac{1}{2}$ has been obtained through the solution of the full Navier–Stokes equations by various authors who considered very different physical situations, i.e. flow with a constant acceleration (Rivero *et al.* 1991; Chang & Maxey 1995), oscillatory flow (Rivero *et al.* 1991; Chang & Maxey 1994), flow with small-amplitude oscillations (Mei, Lawrence & Adrian 1991), steady axisymmetric straining flow (Magnaudet *et al.* 1995), steady flow around a bubble with a time-dependent radius (Legendre, Boree & Magnaudet 1998). In these studies the strength of the acceleration and the Reynolds number covered a very wide range. Moreover most of these studies considered the case of a solid sphere and a recirculating region was present in many cases. The added mass coefficient was always found to be $\frac{1}{2}$ so that there is no doubt that this value is a true constant which depends only on the shape of the body on which the relative normal velocity of the fluid has to vanish. To specify the validity of the equality $C_L = C_M$ it is therefore sufficient to study the variation of the lift coefficient in the high-Reynolds-number limit considered in the present computations.

In §6 we obtained some interesting information about the validity of this equality: since both the analytical result derived in Appendix A and the numerical results demonstrate that the initial value of C_L is $\frac{3}{4}$, it is clear that C_L and C_M differ in strongly unsteady situations, even in the limit $Sr \gg 1$. In §7 we studied the evolution of C_L with Sr in a steady flow and we showed that there is a slight but significant decrease of C_L when Sr is of order unity and that this decrease cannot be attributed to viscous effects. Since no such evolution of C_M with the strength of the acceleration is observed in the works mentioned above, one reaches the conclusion that C_L and C_M are not equal for $Sr = O(1)$. Combining the results found for the transient evolution of C_L with those found for $O(1)$ shear rates, one sees that the equality $C_L = C_M$ holds only in the limit of small shear rates (typically $Sr \leqslant 0.2$ according to present results) and of nearly steady evolutions. These conditions correspond to those of the derivations of Auton (1987), Naciri (1992) and Wells (1993).

9. Summary and conclusions

This paper has been devoted to a quite extensive numerical study of the lift force acting on a clean spherical bubble embedded in a viscous linear shear flow. A wide range of Reynolds number has been explored in order to describe situations dominated by viscous effects as well as nearly inviscid flows. In both asymptotic regimes, systematic comparisons with available analytical solutions have been carried out. Most of the computations reported in this work concerned low to moderate shear rates and steady situations. Nevertheless several simulations dealing with the transient stage of the flow or with higher shear rates have also been carried out. Among the results discussed above the following appear to be especially significant:

(i) The flow field at the surface of the bubble is strongly dependent on the Reynolds

number. At low Re the azimuthal velocity is very small and is directed towards the top of the bubble. When Re increases, the azimuthal velocity first becomes positive close to the front stagnation point. At high Re this velocity is positive over most of the bubble and its strength is one order of magnitude larger than at low Reynolds number. Both the azimuthal and the meridian velocity follow simple azimuthal dependence, except around $Re = 1$.

(ii) At high Reynolds number, the tilting and stretching of the unperturbed spanwise vorticity by the spanwise velocity gradients produced by the presence of the bubble results in a concentration of streamwise vorticity very close to the downstream part of the x-axis. This streamwise vorticity can reach maximum levels much larger than the imposed shear.

(iii) The dominant physical mechanisms governing the lift force are very different at low and high Reynolds number. At high Re, the mechanism is essentially associated with the fact that the vorticity present in the undisturbed flow is distorted asymmetrically by the strain induced by the presence of the bubble. On the other hand, at low Reynolds number the dominant process is associated with the fact that the vorticity generated at the bubble surface diffuses in the flow and is asymmetrically transported by the far-field velocity. Consequently the lift force evolves very differently at low and high Reynolds number. At low Reynolds number the lift coefficient is a decreasing function of Re and it depends strongly on the shear rate. This dependence is quite complex and an empirical correlation has been proposed to describe the evolution of C_L. The lift coefficient reaches a minimum approximately equal to 0.3 around $Re \approx 5$. Beyond this value C_L increases continuously and tends asymptotically towards the value $C_L = 0.5$. In that range of Reynolds number C_L is nearly independent of Sr for low to moderate values of the shear rate.

(iv) The validity of the asymptotic solutions available in the limit of low and high Reynolds number has been specified. At small Reynolds number and moderate to high shear rates, the solution derived by Legendre & Magnaudet (1997) is valid for $Re \leqslant 0.5$ and $Sr/Re \geqslant 0.5$. At high Reynolds number and low to moderate shear rate (i.e. $Sr \leqslant 0.2$) the numerical results are extremely close to Auton's solution $C_L = \frac{1}{2}$ for $Re \geqslant 300$.

(v) The drag force is almost unaffected by the shear rate for $Sr \leqslant 0.2$. In contrast, the simulations carried out at higher shear rate and high Reynolds number demonstrate that the drag is strongly increased when Sr becomes of order unity. More precisely, at high Reynolds number the drag coefficient involves a corrective contribution whose leading term is proportional to $Sr^2\, Re^{-1}$. This increase of the drag force is mainly due to the modifications of the pressure distribution produced by the shear in the front part of the bubble.

(vi) In strongly unsteady situations, like the transient stage which follows the introduction of the bubble in the flow, the lift-coefficient is higher than $\frac{1}{2}$. It has been showed analytically that the initial value of C_L in an inviscid fluid is $\frac{3}{4}$. Similarly, when the Reynolds number is high and the shear rate becomes of order unity, the steady value of C_L decreases slightly but consistently below the value found in the limit of small shear rates.

(vii) The well-known identity $C_L = C_M$ derived by several authors using different starting points has been discussed in some detail. It has been shown that theoretical requirements like frame indifference do not impose any relation between the lift coefficient and the added mass coefficient. Using some of the present computational results it appears that this identity holds only for nearly steady flow when the shear rate is low.

This work was partly supported by a grant from Electricité de France whose help was very much appreciated. Most of the computational time was provided by the Institut pour le Développement des Ressources en Informatique Scientifique (CNRS) where the computations were run on Cray C94 and C98 supercomputers.

Appendix A

In this Appendix we derive analytically the expression for the lift force experienced by a sphere just after its introduction in an inviscid linear shear flow. The notation is that employed in the remainder of the paper except that in place of the angle θ we use the usual meridian angle $\Theta = \pi - \theta$.

Right at the time where the sphere is introduced in the flow, the velocity field $\boldsymbol{V}$ is the sum of the undisturbed field defined by (1) and of an irrotational contribution ensuring that the normal velocity at the surface of the sphere is zero. One can decompose this velocity field into an axisymmetric contribution $\boldsymbol{V}_U$ produced by the uniform velocity U_o and a perturbation $\boldsymbol{V}_0$ resulting from the existence of the shear α.

The axisymmetric velocity field derives from the well-known potential $\Phi_U = U_o(r + R^3/2r^2)\cos\Theta$, so that one has

$$\boldsymbol{V}_U = U_o[(1 - R^3/r^3)\cos\Theta \boldsymbol{e}_r - (1 + R^3/2r^3)\sin\Theta \boldsymbol{e}_\Theta]. \tag{A 1}$$

The perturbation velocity $\boldsymbol{V}_0$ satisfying $\boldsymbol{V}_0 \cdot \boldsymbol{n} = 0$ on the sphere surface ($\boldsymbol{n}$ denoting the local unit normal) may be written in the form $\boldsymbol{V}_0 = \alpha y \boldsymbol{e}_x + \boldsymbol{\nabla}\Phi_0$. One easily finds the potential Φ_0 (see equation (3.1) of Auton 1987), namely

$$\Phi_0 = \frac{\alpha}{6}\frac{R^5}{r^3}\sin 2\Theta \cos\phi. \tag{A 2}$$

At very short time, i.e. $t \quad t_a = R/U_o$, the vorticity equation is then

$$\frac{\partial \boldsymbol{\omega}}{\partial t} + (\boldsymbol{V}_U + \boldsymbol{V}_0)\cdot\boldsymbol{\nabla}\boldsymbol{\omega}_0 = \boldsymbol{\omega}_0 \cdot \boldsymbol{\nabla}(\boldsymbol{V}_U + \boldsymbol{V}_0). \tag{A 3}$$

Since the initial vorticity $\boldsymbol{\omega}_0 = \boldsymbol{\nabla} \times \boldsymbol{V}_0 = -\alpha \boldsymbol{e}_z$ is uniform, the advective term is zero. Moreover, in the limit $Sr \quad 1$, $\boldsymbol{V}_0$ is much smaller than $\boldsymbol{V}_U$ and can be neglected in (A 3). Thus the solution of (A 3) is simply

$$\boldsymbol{\omega}(t) = \boldsymbol{\omega}_0 + t\boldsymbol{\omega}_0 \cdot \boldsymbol{\nabla}\boldsymbol{V}_U + O(\alpha Sr\, t/t_a, \alpha(t/t_a)^2). \tag{A 4}$$

The second term on the right-hand side of (A 4) produces an additional velocity field $\boldsymbol{V}_1$ which grows linearly in time and satisfies the conditions

$$\left.\begin{aligned} &\boldsymbol{\nabla}\cdot\boldsymbol{V}_1 = 0, \\ &\boldsymbol{\nabla}\times\boldsymbol{V}_1 = t\boldsymbol{\omega}_0\cdot\boldsymbol{\nabla}\boldsymbol{V}_U, \\ &\boldsymbol{V}_1\cdot\boldsymbol{n} = 0 \quad \text{for} \quad r = R, \\ &\boldsymbol{V}_1 \to 0 \quad \text{as} \quad r \to \infty. \end{aligned}\right\} \tag{A 5}$$

The complete velocity field around the sphere is thus at very short time $\boldsymbol{V} = \boldsymbol{V}_U + \boldsymbol{V}_0 + \boldsymbol{V}_1$. Taking into account the fact that $\boldsymbol{V}_1$ is initially zero, for $t \quad t_a$ the Euler equation is

$$\frac{\partial \boldsymbol{V}_1}{\partial t} + \boldsymbol{\omega}_0 \times (\boldsymbol{V}_U + \boldsymbol{V}_0) + \tfrac{1}{2}\boldsymbol{\nabla}(\boldsymbol{V}_U + \boldsymbol{V}_0)^2 = -\frac{1}{\rho}\boldsymbol{\nabla}(P_U + \mathscr{P}), \tag{A 6}$$

where P_U is the pressure field associated with $\boldsymbol{V}_U$. Since this pressure field does not

produce any force, the lift force is entirely determined by the distribution of $\mathscr{P}$ on the sphere. Using these approximations, the governing equation of the leading contribution to $\mathscr{P}$, say $\mathscr{P}_1$, is

$$\frac{\partial \boldsymbol{V}_1}{\partial t}+\boldsymbol{\omega}_0\times \boldsymbol{V}_U+\boldsymbol{\nabla}(\boldsymbol{V}_U\cdot \boldsymbol{V}_0)=-\frac{1}{\rho}\boldsymbol{\nabla}\mathscr{P}_1. \tag{A 7}$$

Since $\boldsymbol{V}_U$ and $\boldsymbol{V}_0$ are known from (A 1) and (A 2) it is clear from (A 7) that the key step for calculating the initial value of the lift force is the solution of the problem (A 5). Using (A 1) one first obtains the expression for the vortex stretching term in spherical coordinates, namely

$$\boldsymbol{\omega}_0\cdot\boldsymbol{\nabla}\boldsymbol{V}_U=-\tfrac{3}{2}\alpha U_o\frac{R^3}{r^4}[\sin\phi(\tfrac{3}{2}\sin 2\Theta\boldsymbol{e}_r-\cos 2\Theta)\,\boldsymbol{e}_\Theta-\cos\Theta\cos\phi\boldsymbol{e}_\phi]. \tag{A 8}$$

The rotational part of $\boldsymbol{V}_1$, say $\boldsymbol{V}_{1R}$, is governed by the first and the second equations of (A 5). Expressing $\boldsymbol{\nabla}\times\boldsymbol{V}_{1R}$ in spherical coordinates and using (A 8) one finds after some calculations that $\boldsymbol{V}_{1R}$ is given by

$$\boldsymbol{V}_{1R}=-\tfrac{3}{2}\alpha U_o\,t\frac{R^3}{r^3}[\sin\Theta\cos\phi\boldsymbol{e}_r+\sin^2\Theta\sin\phi\boldsymbol{e}_\phi]. \tag{A 9}$$

Equation (A 9) shows that $\boldsymbol{V}_{1R}$ induces a non-zero radial velocity $-\tfrac{3}{2}\alpha U_o\,t\sin\Theta\cos\phi$ at the surface of the sphere. Thus this solution must be completed by an irrotational velocity field $\boldsymbol{V}_{1P}$ so that $\boldsymbol{V}_1=\boldsymbol{V}_{1R}+\boldsymbol{V}_{1P}$ satisfies the third condition in (A 5). One finds easily that the potential Φ_1 which gives $\boldsymbol{V}_{1P}=\boldsymbol{\nabla}\Phi_1$ is

$$\Phi_1=-\tfrac{3}{4}\alpha U_o\,t\frac{R^3}{r^2}\sin\Theta\cos\phi. \tag{A 10}$$

Using (A 9) and (A 10) one finally gets the expression for the perturbation velocity $\boldsymbol{V}_1$ induced by the vortex stretching mechanism, namely

$$\boldsymbol{V}_1=-\tfrac{3}{4}\alpha U_o\,t\frac{R^3}{r^3}[\cos\Theta\cos\phi\boldsymbol{e}_\Theta-\cos 2\Theta\sin\phi\boldsymbol{e}_\phi]. \tag{A 11}$$

One can now integrate the momentum equation (A 7) in order to obtain the pressure $\mathscr{P}_1$. Using (A 1), (A 2) and (A 11) one obtains on the sphere

$$\mathscr{P}_1(r=R,\Theta,\phi)=\mathscr{P}_0+\tfrac{5}{4}\rho\alpha U_o\,R\sin\Theta\cos 2\Theta\cos\phi, \tag{A 12}$$

where $\mathscr{P}_0$ is a constant. Finally the lift force at very short time, say $F_L(t=0^+)$, is obtained by evaluating the integral

$$F_L(t=0^+)=-\int\mathscr{P}_1(r=R,\Theta,\phi)\,\boldsymbol{n}\cdot\boldsymbol{e}_y\,\mathrm{d}S=-R^2\int\mathscr{P}_1(r=R,\Theta,\phi)\sin^2\Theta\cos\phi\,d\Theta\,\mathrm{d}\phi. \tag{A 13}$$

One gets

$$F_L(t=0^+)=\pi\rho R^3\alpha U_o \tag{A 14}$$

which yields, using the definition (6)

$$C_L(t=0^+)=\tfrac{3}{4}. \tag{A 15}$$

This result shows that the initial lift coefficient is larger by one half than its steady value. This finding suggests that the advection of vorticity which does not contribute to the solution (A 15) decreases the value of C_L because it tends to make the disturbed flow more symmetric.

The above result has been derived under the assumption that the shear is weak. However, it is straightforward to show that (A 15) holds whatever the value of Sr. For that purpose let us come back to (A 3). If the vortex stretching term $\boldsymbol{\omega}_0 \cdot \boldsymbol{\nabla} \boldsymbol{V}_0$ is no longer neglected, the vorticity equation produces an additional velocity field $\boldsymbol{V}_2$ satisfying at short time the conditions

$$\left.\begin{aligned} &\boldsymbol{\nabla} \cdot \boldsymbol{V}_2 = 0, \\ &\boldsymbol{\nabla} \times \boldsymbol{V}_2 = t \boldsymbol{\omega}_0 \cdot \boldsymbol{\nabla} \boldsymbol{V}_0, \\ &\boldsymbol{V}_2 \cdot \boldsymbol{n} = 0 \quad \text{for} \quad r = R, \\ &\boldsymbol{V}_2 \to 0 \quad \text{as} \quad r \to \infty. \end{aligned}\right\} \tag{A 16}$$

The complete velocity field around the sphere is now $\boldsymbol{V} = \boldsymbol{V}_U + \boldsymbol{V}_0 + \boldsymbol{V}_1 + \boldsymbol{V}_2$ and the additional pressure field $\mathscr{P}_2$ associated with the nonlinear effects of the shear is governed at very short time by

$$\frac{\partial \boldsymbol{V}_2}{\partial t} + \boldsymbol{\omega}_0 \times \boldsymbol{V}_0 + \tfrac{1}{2} \boldsymbol{\nabla} \boldsymbol{V}_0^2 = -\frac{1}{\rho} \boldsymbol{\nabla} \mathscr{P}_2. \tag{A 17}$$

Equation (A 17) is identical to the momentum balance corresponding to a velocity $\boldsymbol{V}_F = \alpha y \boldsymbol{e}_x$ far from the sphere, i.e. to a pure shear flow with a zero velocity at the centre of the sphere. In such a situation, no lift force can exist for obvious symmetry reasons. Hence one concludes immediately that $\mathscr{P}_2$ does not contribute to the lift force, so that (A 15) holds whatever the value of Sr.

Finally, it is interesting to extend the foregoing analysis to another simple case of rotational flow, namely the purely rotating flow defined by

$$\boldsymbol{V} = (U_o + \tfrac{1}{2} \alpha y) \, \boldsymbol{e}_x - \tfrac{1}{2} \alpha x \boldsymbol{e}_y. \tag{A 18}$$

This flow has the same initial vorticity $\boldsymbol{\omega}_0 = -\alpha \boldsymbol{e}_z$ as the pure shear flow considered before. Since the axisymmetric velocity field $\boldsymbol{V}_U$ is also similar in both flows, it results from (A 4) and (A 5) that the velocity contribution $\boldsymbol{V}_1$ is still given by (A 11) in this second flow. Thus for the present problem the only difference between the two flows lies in the velocity perturbation $\boldsymbol{V}_0$. Since the unperturbed rotating flow does not induce any normal velocity at the surface of the sphere, the corresponding value of $\boldsymbol{V}_0$, say $\boldsymbol{V}_0'$, is simply given by

$$\boldsymbol{V}_0' = \tfrac{1}{2} \alpha (y \boldsymbol{e}_x - x \boldsymbol{e}_y). \tag{A 19}$$

By replacing $\boldsymbol{V}_0$ by $\boldsymbol{V}_0'$ in (A 7) one finds immediately that the various terms of the left-hand side cancel, so that the pressure perturbation $\mathscr{P}$ at the surface of the sphere obeys

$$\boldsymbol{\nabla} \mathscr{P}'(r = R, \Theta, \phi) = 0 \tag{A 20}$$

which yields

$$C_{LR}(t = 0^+) = 0, \tag{A 21}$$

where $C_{LR}(t = 0^+)$ is the initial value of the lift coefficient in the present flow. Combining this result with (A 15) shows that the usual relation $C_{LR} = C_L - \frac{1}{2}(1 + C_M)$ linking the so-called rotational lift coefficient C_{LR} to the shear lift coefficient C_L and to the added mass coefficient C_M (see Auton *et al.* 1988) is still valid, at least at very short time, for a strongly unsteady, three-dimensional inviscid flow. The case of a sphere moving arbitrarily in a time-dependent straining flow in solid body rotation was considered by Drew & Lahey (1987, 1990) who used a frame of reference rotating with the flow. In their original derivation these authors assumed erroneously that the flow seen in the rotating frame was irrotational at all time, i.e. that the contribution equivalent to $\boldsymbol{V}_1$ was zero. In their corrigendum (Drew & Lahey 1990), they recognized

the existence of $\boldsymbol{V}_1$ but avoided its calculation by using a method giving directly the force in terms of the normal pressure gradient $\boldsymbol{n}\cdot\boldsymbol{\nabla}\mathscr{P}'$ at the surface of the sphere. It is straightforward to see in (A 7) that at short time $\boldsymbol{n}\cdot\boldsymbol{\nabla}\mathscr{P}'$ does not involve $\boldsymbol{V}_1$, owing to the condition $\boldsymbol{V}_1\cdot\boldsymbol{n}=0$ on the sphere. Consequently the original result of Drew & Lahey (1987) is correct at short time. This means that the result they obtained (in the particular case where the flow in the inertial frame is steady and has a zero strain rate and where the sphere is at rest at the origin of the coordinate system) must be equivalent to the result (A 21). To prove that this is indeed the case, it is convenient to use (B 1) of Appendix B. If the flow defined by (A 18) is studied in a frame of reference rotating with the angular velocity $\boldsymbol{\Omega}=-\alpha\boldsymbol{e}_z$, the observer sees a uniform time-dependent flow. Thus, recognizing that in the rotating frame the generalized buoyancy force $\boldsymbol{F}_o^*$ equals $\rho\mathscr{V}[\mathrm{d}\boldsymbol{U}^*/\mathrm{d}t+2\boldsymbol{\Omega}\times\boldsymbol{U}^*]$ (if gravity is neglected), (B 1) reduces to

$$\boldsymbol{F}^*=\rho\mathscr{V}\left[\frac{\mathrm{d}\boldsymbol{U}^*}{\mathrm{d}t}+2\boldsymbol{\Omega}\times\boldsymbol{U}^*+C_M\frac{\mathrm{d}\boldsymbol{U}^*}{\mathrm{d}t}+2(C_L-C_M)\,\boldsymbol{U}^*\times\boldsymbol{\Omega}\right]. \tag{A 22}$$

By inserting $C_L=3/4$ and $C_M=1/2$ in (A 22), it is immediately obvious that the result (A 22) is equivalent to equation (45) of Drew & Lahey (1987) (after correcting the sign of the Coriolis force in the latter equation). Moreover, noting that $\mathrm{d}\boldsymbol{U}^*/\mathrm{d}t=-\boldsymbol{\Omega}\times\boldsymbol{U}^*$, one finds that (A 22) yields $\boldsymbol{F}^*=0$, i.e. that it is equivalent to the result (A 21) as it must be. Surprisingly, Drew & Lahey (1987, 1990) claimed that their result was equivalent to Auton's result $C_L=\frac{1}{2}$, or in other words that their derivation supported the identity $C_L=C_M$. This erroneous conclusion was due to several errors made in the transformation of velocities and accelerations between the rotating frame and the fixed one. Equations (A 21) and (A 22) clarify the situation in showing that the result found by Drew & Lahey (1987, 1990) is equivalent to our result $C_L(t=0^+)=\frac{3}{4}$ but *not* to the result $C_L=\frac{1}{2}$ obtained by Auton in a steady flow.

Appendix B

In this Appendix we indicate how the hydrodynamic force acting on a sphere moving in an inviscid, weakly rotational flow can be expressed in a rotating frame of reference and we show that this expression does not give any indication about the value of the lift coefficient or its relation to the added mass coefficient. We start from the particular case where the flow in the inertial frame is irrotational, because this situation was already considered by Zhang & Prosperetti (1994). In that case, if one considers separately the generalized buoyancy force $\boldsymbol{F}_o$ applied on the volume $\mathscr{V}$ of the sphere by the unperturbed flow, i.e. $\boldsymbol{F}_o=\rho\mathscr{V}(\mathrm{D}\boldsymbol{U}/\mathrm{D}t-\boldsymbol{g})$ ($\boldsymbol{g}$ denoting the acceleration due to gravity), the only force acting on the sphere in the inertial frame is the added mass force which is proportional to $\boldsymbol{A}=C_M(\mathrm{D}\boldsymbol{U}/\mathrm{D}t-\mathrm{d}\boldsymbol{U}_d/\mathrm{d}t)$, where $\mathrm{D}\boldsymbol{U}/\mathrm{D}t$ denotes the local acceleration of the fluid while $\mathrm{d}\boldsymbol{U}_d/\mathrm{d}t$ is the time-derivative of the sphere velocity $\boldsymbol{U}_d$ following its own motion (see Auton *et al.* 1988). Zhang & Prosperetti pointed out correctly that this expression for $\boldsymbol{A}$ cannot be used in a frame rotating with the angular velocity $\boldsymbol{\Omega}$ because the flow is no longer irrotational in that case. To overcome this limitation they added a complementary term $\boldsymbol{X}$ to $\boldsymbol{A}$ and they determined $\boldsymbol{X}$ in such a way that the total force satisfies the OFI principle, i.e. that it transforms objectively from one frame of reference to another. Since $\boldsymbol{A}$ can be expressed in terms of the quantities evaluated in the rotating frame (denoted with a star) in the form $\boldsymbol{A}=C_M[\mathrm{D}^*\boldsymbol{U}^*/\mathrm{D}t-\mathrm{d}^*\boldsymbol{U}_d^*/\mathrm{d}t-2(\boldsymbol{U}^*-\boldsymbol{U}_d^*)\times\boldsymbol{\Omega}]$, Zhang & Prosperetti (see Appendix B 3 of their paper) showed that the correct expression for $\boldsymbol{X}$ is $\boldsymbol{X}=-2C_M(\boldsymbol{U}^*-\boldsymbol{U}_d^*)\times\boldsymbol{\Omega}$ which accounts for the effect of Coriolis acceleration. Since in the rotating frame the

fluid has a uniform vorticity $\boldsymbol{\omega}^* = -2\boldsymbol{\Omega}$, $\boldsymbol{X}$ has the form of the lift force found by Auton (1987) provided one defines a 'lift' coefficient $C_L^* = C_M$. On these grounds Zhang & Prosperetti (1994) identified both forces. However, it must be stressed that the above result was obtained in the very particular case where the absolute vorticity $\boldsymbol{\omega}_a = \boldsymbol{\omega}^* + 2\boldsymbol{\Omega}$ is zero. Let us now extend the foregoing derivation to the more general case where the vorticity $\boldsymbol{\omega} = \boldsymbol{\omega}_a$ is small but non-zero in the initial frame. For that purpose the above form of $\boldsymbol{A}$ must be replaced by $\boldsymbol{B} = \boldsymbol{A} + C_L(\boldsymbol{U} - \boldsymbol{U}_d) \times \boldsymbol{\omega}$ which is the expression for the force found by Auton *et al.* (1988). To make this expression valid in a rotating frame and to satisfy the OFI principle, it is straightforward to show by using the usual transformation rules (see Appendix B 3 of Zhang & Prosperetti 1994) that the corrective term $\boldsymbol{X}$ must be replaced by $\boldsymbol{Y} = 2(C_L - C_M)(\boldsymbol{U}^* - \boldsymbol{U}_d^*) \times \boldsymbol{\Omega}$. Thus in the rotating frame the objective expression for the total force $\boldsymbol{F}^*$ experienced by the sphere under the assumptions considered by Auton *et al.* is

$$\frac{\boldsymbol{F}^* - \boldsymbol{F}_0^*}{\rho \mathscr{V}} = C_M \left[\frac{\mathrm{D}^* \boldsymbol{U}^*}{\mathrm{D}t} - \frac{\mathrm{d}^* \boldsymbol{U}_d^*}{\mathrm{d}t} \right] + C_L(\boldsymbol{U}^* - \boldsymbol{U}_d^*) \times \boldsymbol{\omega}^* + 2(C_L - C_M)(\boldsymbol{U}^* - \boldsymbol{U}_d^*) \times \boldsymbol{\Omega}. \tag{B 1}$$

It can easily be checked by considering various basic flows that the magnitude of $\boldsymbol{F}^*$ predicted by (B 1) is independent of the frame of reference of the observer as it must be. As already pointed out, in the particular case considered by Zhang & Prosperetti the absolute vorticity is identically zero. Consequently one sees immediately in (B 1) that the terms involving C_L cancel exactly, whatever the value of C_L. The means that the term $\boldsymbol{X}$ derived by Zhang & Prosperetti must not be confused with the lift force derived by Auton (1987): the two terms are completely distinct and in that case the 'identity' $C_L^* = C_M$ is just a definition which has nothing to do with Auton's result. If instead of a sphere one considers the two-dimensional flow around a circular cylinder for which it is well known that $C_M = 1$ and $C_L = 2$ (see Batchelor 1967, p. 543), there is no more possible confusion between C_L and C_L^*. In other words, the OFI principle does not tell us anything about the lift coefficient C_L. It just shows that *if* $C_L = C_M$, (B 1) has a form identical to the expression established by Auton *et al.* (1988) in a fixed frame of reference.

REFERENCES

Auton, T. R. 1984 The dynamics of bubbles, drops and particles in motion in liquids. PhD Dissertation, University of Cambridge.

Auton, T. R. 1987 The lift force on a spherical body in a rotational flow. *J. Fluid Mech.* **183**, 199–218.

Auton, T. R., Hunt, J. C. R. & Prud'homme, M. 1988 The force exerted on a body in inviscid unsteady non-uniform rotational flow. *J. Fluid Mech.* **197**, 241–257.

Batchelor, G. K. 1967 *An Introduction to Fluid Dynamics*. Cambridge University Press.

Blanco, A., & Magnaudet, J. 1995 The structure of the high Reynolds number flow around an ellipsoidal bubble of fixed shape. *Phys. Fluids* **7**, 1265–1274.

Calmet, I. & Magnaudet, J. 1997 Large-eddy simulation of high Schmidt number mass transfer in a turbulent channel flow. *Phys. Fluids* **9**, 438–455.

Chang, E. J. & Maxey, M. R. 1994 Unsteady flow about a sphere at low to moderate Reynolds number. Part 1. Oscillatory motion. *J. Fluid Mech.* **277**, 347–379.

Chang, E. J. & Maxey, M. R. 1995 Unsteady flow about a sphere at low to moderate Reynolds number. Part 2. Accelerated motion. *J. Fluid Mech.* **303**, 133–153.

Cousins, R. R. 1970 A note on the shear flow past a sphere. *J. Fluid Mech.* **40**, 543–547.

Cuenot, B., Magnaudet, J. & Spennato, B. 1997 The effects of slightly soluble surfactants on the flow around a spherical bubble. *J. Fluid Mech.* **339**, 25–53.

Dandy, D. S. & Dwyer, H. A. 1990 A sphere in shear flow at finite Reynolds number: effect of shear on particle lift, drag, and heat transfer. *J. Fluid Mech.* **216**, 381–410.

Darwin, C. 1953 Note on hydrodynamics. *Camb. Phil. Trans.* **49**, 342–354.

Drew, D. & Lahey, R. T. 1979 Applications of general constitutive principles to the derivation of multidimensional two-phase flow equations. *Intl J. Multiphase Flow* **5**, 243–264.

Drew, D. & Lahey, R. T. 1987 The virtual mass and lift force on a sphere in rotating and straining inviscid flow. *Intl J. Multiphase Flow* **13**, 113–121.

Drew, D. & Lahey, R. T. 1990 Some supplemental analysis concerning the virtual mass and lift force on a sphere in a rotating and straining flow. *Intl J. Multiphase Flow* **16**, 1127–1130.

Eames, I., Belcher, S. E. & Hunt, J. C. R. 1994 Drift, partial drift and Darwin's proposition. *J. Fluid Mech.* **275**, 201–223.

Ervin, E. A. & Tryggvason, G. 1994 The rise of bubbles in a vertical shear flow. *Proc. ASME Winter Meeting, Fluids Engng Div., Chicago.*

Hall, I. M. 1956 The displacement effect of a sphere in a two-dimensional flow. *J. Fluid Mech.* **1**, 142–161.

Harper, E. Y. & Chang, I. D. 1968 Maximum dissipation resulting from lift in a slow viscous shear flow. *J. Fluid Mech.* **33**, 209–225.

Komori, S. & Kurose, R. 1996 The effects of shear and spin on particle lift and drag in shear flow at high Reynolds numbers. *Advances in Turbulence VI* (ed. S. Gavrilakis, L. Machiels & P. Monkewitz), pp. 551–554. Kluwer.

Kurose, R. & Komori, S. 1997 Drag and lift forces on a rotating sphere in a linear shear flow. *J. Fluid Mech.* (submitted).

Lamb, H. 1932 *Hydrodynamics*, 6th Edn. Cambridge University Press.

Legendre, D. 1996 Quelques aspects des forces hydrodynamiques et des transferts de chaleur sur une bulle sphérique. Thèse de Doctorat, Inst. Nat. Polytech. de Toulouse, Toulouse.

Legendre, D., Boree, J. & Magnaudet, J. 1998 Thermal and dynamic aspects of the evolution of a spherical bubble moving steadily in a superheated or subcooled liquid. *Phys. Fluids* **10** (in press).

Legendre, D. & Magnaudet, J. 1997 A note on the lift force on a bubble or a drop in a low-Reynolds-number shear flow. *Phys. Fluids* **9**, 3572–3574.

Levich, V. G. 1962 *Physicochemical Hydrodynamics.* Prentice Hall.

Lighthill, M. J. 1956 *J. Fluid Mech.* **1**, 31–53 and corrigendum *J. Fluid Mech.* **2** (1957), 311.

Magnaudet, J. 1997 The forces acting upon bubbles and rigid particles. *Proc. ASME Summer Meeting, Fluids Engng Div., Vancouver.*

Magnaudet, J. & Legendre, D. 1998 Some aspects of the lift force on a spherical bubble. *Flow, Turbulence and Combustion.* Special issue in honour of L. Van Wijngaarden (in press).

Magnaudet, J., Rivero, M. & Fabre, J. 1995 Accelerated flows past a rigid sphere or a spherical bubble. Part 1. Steady straining flow. *J. Fluid Mech.* **284**, 97–135.

Mei, R., Lawrence, C. J. & Adrian, R. J. 1991 Unsteady drag on a sphere at finite Reynolds number with small-amplitude fluctuations in the free-stream velocity. *J. Fluid Mech.* **233**, 613–631.

McLaughlin, J. B. 1991 Inertial migration of a small sphere in linear shear flows. *J. Fluid Mech.* **224**, 261–274.

Moore, D. W. 1963 The boundary layer on a spherical gas bubble. *J. Fluid Mech.* **16**, 161–176.

Naciri, A. 1992 Contribution à l'étude des forces exercées par un liquide sur une bulle de gaz: portance, masse ajoutée et interactions hydrodynamiques. Thèse de Doctorat, Ec. Centrale de Lyon, France.

Rivero, M., Magnaudet, J. & Fabre, J. 1991 Quelques résultats nouveaux concernant les forces exercées sur une inclusion sphérique par un écoulement accéléré. *C. R. Acad. Sci. Paris* II, **312**, 1499–1506.

Rubinow, S. I. & Keller, J. B. 1961 The transverse force on a spinning sphere moving in a viscous fluid. *J. Fluid Mech.* **11**, 447–459.

Ryskin, G. & Rallison, J. M. 1980 On the applicability of the approximation of material frame indifference in suspension mechanics. Appendix to Ryskin, G. 1980 The extensional viscosity of a dilute suspension of spherical particles at intermediate microscale Reynolds numbers. *J. Fluid Mech.* **99**, 513–529.

Saffman, P. G. 1965 The lift force on a small sphere in a slow shear flow. *J. Fluid Mech.* **22**, 385–400 and corrigendum *J. Fluid Mech.* **31** (1968), 624.

Segré, G. & Silberberg, A. 1962*a* Behaviour of macroscopic rigid spheres in Poiseuille flow. Part 1. *J. Fluid Mech.* **14**, 115–135.

Segré, G. & Silberberg, A. 1962*b* Behaviour of macroscopic rigid spheres in Poiseuille flow. Part 2. *J. Fluid Mech.* **14**, 136–157.

Takagi, S. & Matsumoto, Y. 1995 Three-dimensional calculation of a rising bubble. *Proc. 2nd Int. Conf. on Multiphase Flow*, *Kyoto*.

Taylor, T. D. & Acrivos, A. 1964 On the deformation and drag of a falling viscous drop at low Reynolds number. *J. Fluid Mech.* **18**, 466–476.

Wells, J. C. 1993 A geometrical interpretation of lift on bubbles in shear flow. *Proc. Conf. on Gas–Liquid Flows*, *ASME Fluids Engng Div.*, *Washington DC*.

Wells, J. C. 1996 A geometrical interpretation of force on a translating body in rotational flow. *Phys. Fluids* **8**, 442–450.

Zhang, D. Z. & Prosperetti, A. 1994 Averaged equations for inviscid disperse two-phase flow. *J. Fluid Mech.* **267**, 185–219.